USING SPONTANEOUS IMBIBITION AND MERCURY INTRUSION POROSIMETRY TO INVESTIGATE THE EFFECT OF PORE STRUCTURE ON FLUID MIGRATION WITHIN POROUS MEDIA

by

ZHIYE GAO

Presented to the Faculty of the Graduate School of
The University of Texas at Arlington in Partial Fulfillment
of the Requirements
for the Degree of

DOCTOR OF PHILOSOPHY

THE UNIVERSITY OF TEXAS AT ARLINGTON
May 2014

Acknowledgements

I would like to thank my research advisor, Dr. Qinhong Hu, for his support and guidance during my graduate studies.

I greatly appreciate the assistance of all the committee members (Dr. James P. Grover, Dr. Andrew Hunt, Dr. William A. Griffith and Dr. Hyeok Choi).

I would also like to express my gratitude to the funding agencies in my research. The research in Chapter 2 was supported by Lawrence Livermore National Laboratory (LNNL), Livermore, CA. The research in Chapters 3-6 was supported by the Student Research Grant from Gulf Coast Association of Geological Societies, and RPSEA through the "Ultra-Deepwater and Unconventional Natural Gas and Other Petroleum Resources" program authorized by the U.S. Energy Policy Act of 2005.

Last but not least, I would especially like to thank my parents, mother Xiuying Gao and father Liangsong Gao, for their continuing support in my life.

April 15, 2014

Abstract

USING SPONTANEOUS IMBIBITION AND MERCURY INTRUSION POROSIMETRY TO INVESTIGATE THE EFFECT OF PORE STRUCTURE ON FLUID MIGRATION WITHIN POROUS MEDIA

Zhiye Gao, PhD

The University of Texas at Arlington, 2014

Supervising Professor: Qinhong Hu

Much research has been conducted to investigate the property of fluid (water/oil/gas) migration in different types of porous media, and the knowledge of pore structure (including pore geometry and pore connectivity) plays an important role in this research. This dissertation will characterize the pore structure of different porous media (including building materials and natural rocks) by using spontaneous imbibition and mercury intrusion porosimetry (MIP).

A new approach to deriving effective permeability of building materials using imbibition experiments is provided. Spontaneous imbibition is an important process in oil/gas production and its rate could affect oil/gas recovery rate significantly. As a result, this study performs spontaneous imbibition experiments using two types of imbibing fluids (water/n-decane) on the reservoir rocks to investigate their imbibition behaviors. Also, directional spontaneous imbibition is conducted on Barnett shale samples because of their layered characteristics and wettability information is indicated from these imbibition experiments.

MIP has been successfully applied to characterize the pore-throat size distribution of porous media for several decades, and several important parameters, including permeability, gas diffusion coefficient and tortuosity, are derived from the resultant pore-throat size distribution in this dissertation. Our results indicate that the median pore-throat diameter (d_{50}), which is defined as the pore-throat diameter corresponding to 50% mercury saturation during MIP measurement, plays an important role in both gas diffusion and spontaneous imbibition processes.

Table of Contents

List of Illustrations

List of Tables

Chapter 1

Introduction

Many scientists and engineers have recognized the importance of pore structure research, because it plays an important role in controlling fluid transport in porous media. Hu et al. [40] characterized the pore connectivity of natural rocks using spontaneous water imbibiton, tracer concentration profiles, and imaging in combination with network modeling. Gao and Hu [28] proposed an empirical equation solely using median pore-throat radius (r_{50}) to calculate permeability, which is an important hydraulic parameter, and the sole use of r_{50} to predict permeability indicated that the fluid transport in porous media may be controlled by median pore-throat radius.

Nowadays more and more unconventional hydrocarbon reservoirs with extremely low permeability have been explored due to the maturity of drilling and completion technology, especially the development of horizontal drilling and hydraulic fracturing. Much research has been conducted to characterize these reservoirs from different perspectives. Chalmers et al. [14] investigated the pore systems of Barnett shale using multiple approaches, including mercury intrusion porosimetry (MIP). Loucks et al. [51] discussed spectrum of pore types and networks in mudrocks and proposed a descriptive classification for matrix-related mudrock pores.

In this dissertation, I will focus on characterizing the pore structure of different porous media (including building materials and natural rocks) using spontaneous imbibition (SI) and mercury intrusion porosimetry (MIP). Pore-throat size distribution is the main information obtained from MIP and many important parameters (e.g. permeability, gas diffusivity) could be derived from MIP data. Also I will try to interpret the effects of pore structure on fluid migration by combining the pore structure information obtained from MIP with imbibition results.

1.1 Spontaneous Imbibition

Spontaneous imbibition (SI) is a capillary-force controlled process during which a wetting fluid displaces the non-wetting fluid by capillary force only, and it plays an important role in gas/oil recovery of fractured reservoirs. In the process of oil/gas recovery from fractured reservoirs, water is imbibed into the rock matrix blocks from the fracture system by SI, with the result that oil /gas in the matrix is displaced by the water. As a result, the oil/gas production rate is strongly dependent on the SI process, and extensive research has been undertaken to investigate that process [32, 47, 76, 80].

Handy [34] proposed the following equation (Eq. (1-1)) to describe the SI process in a water-air system in which imbibition occurs vertically upward and the gravitational force can be neglected:

$$Q_w^2 = (\frac{2P_c k_w \emptyset A^2 S_w}{\mu_w})t \tag{1-1}$$

where Q_w is the volume of water imbibed into the core sample in cm^3; P_c is the capillary pressure (atm); k_w is the effective permeability in darcies; $\emptyset$ is fractional porosity; A is the cross-sectional area of the core in cm^2; S_w is fractional water content of the pore spaces; t is imbibition time in seconds; and μ_w is the viscosity of water in centipoises.

Handy's equation (Eq. (1-1)) is based on three assumptions (1) the water imbibes in a piston-like manner; (2) the pressure gradient in the gas phase ahead the water front can be neglected; and (3) gravity forces are much less than capillary forces. In piston-like displacement, all capillaries fill at the same time leaving a residual gas saturation behind and the capillary forces at the front were assumed to provide the driving force to overcome viscous flow throughout the porous medium in which water is flowing. Handy's equation implies that the cumulative imbibition is proportional to the square root of the imbibition time, so that theoretically a slope of 0.5 should be obtained if cumulative imbibition is plotted vs. imbibition time on log-log coordinates. Percolation theory suggests that the lower slope values may be an indication of low pore connectivity [40].

Wettability, boundary conditions, shape factor, viscosities of fluids, interfacial tension, initial wetting fluid saturation, pore structure of the rock, and temperature are generally considered the important factors influencing the imbibition process [57, 62, 89]. Scaling of SI behavior is generally recognized as an effective method of investigating the factors controlling the SI process. The following scaling equation is widely used in petroleum engineering [55, 58, 90],

$$t_D = t\sqrt{\frac{k}{\emptyset}}\frac{\sigma}{\sqrt{\mu_{we}\mu_{nw}}L_c^2} \tag{1-2}$$

Where t_D is dimensionless time; t is imbibition time (s); k is absolute permeability (m^2); $\emptyset$ is fractional pososity; σ is interfacial tension (N/m) between wetting and non-wetting phases; μ_{we} is the viscosity of the wetting phase (Pa•s); μ_{nw} is the viscosity of the non-wetting phase (Pa•s); L_c is the characteristic length (m).

As mentioned by Li [47], the limitations of Eq. (1-2) include that (1) wettability must be the same; (2) relative permeability functions must be identical; (3) capillary pressure functions must be identically proportional to interfacial tension; (4) initial fluid distributions must be duplicated; and (5) gravity must be neglected.

By using Eq. (1-2), imbibition data can be adjusted to compensate for differences in pore structure, viscosity, interfacial tension and boundary conditions; wettability, the remaining factor, is not taken into account when the imbibition of different fluids into the same sample is considered. As a result, for the same sample the difference of imbibition behavior is mainly determined by wettability after scaling with Eq. (1-2).

1.2 Mercury Intrusion Porosimetry

Over the past 30 years, mercury intrusion porosimetry (MIP) has become a well-established technique for characterizing porous media, since Washburn [86] proposed the relationship between capillary pressure and the pore radius as the basic theory for MIP. Compared with other pore size characterization approaches (e.g. gas sorption), MIP based on a simpler principle could cover a wide range of pore sizes (from 3nm to 300 μm), which makes it a powerful characterization tool. Also MIP is less time consuming, one MIP test is usually completed within 1 hour for not-so-tight samples like sandstones and carbonates, for shale samples it usually needs two hours because of long evacuation time due to its nano-sized pores during low pressure analysis.

As a non-wetting fluid to most porous media, mercury will not invade pores unless external pressure is applied. The diameter of the pores invaded by mercury is inversely proportional to the applied pressure; the higher pressure is applied, the smaller pores will be invaded by mercury. Washburn [86] developed the following equation based on the assumption that all the pores are cylindrical,

$$\Delta P = -\frac{2\gamma cos\theta}{R} \tag{1-3}$$

Where ΔP is the pressure difference across the curved mercury interface; γ is the surface tension of mercury; θ is the contact angle between mercury and the porous medium; R is the corresponding pore-throat radius.

Permeability is an important parameter to characterize the easiness of a reservoir to transmit hydrocarbons, and accurate measurement or estimation of permeability has been a challenging task. Due to the limitations (e.g., required experimental apparatus and long duration, especially for tight samples) associated with the permeability measurement, several empirical relationships have been published to predict permeability based on other parameter(s) that are relatively easy to obtain.

Purcell [68] related air permeability to capillary pressure by the graphical integral of the curve of mercury saturation versus reciprocal capillary pressure squared. Swanson [82] presented a new equation which related permeability empirically to the hyperbola of the log-log mercury intrusion capillary pressures curve as follows,

$$k_{air} = 339(S_{HG}/P_c)_{apex}^{1.691} \tag{1-4}$$

Where k_{air} is air permeability (mD), S_{HG} is the mercury saturation (%) corresponding to the apex of the hyperbola and P_c is capillary pressure (psi).

Katz and Thompson [42, 43] developed two equations for predicting air permeability (*k*) based on the MIP data.

$$k = \frac{1}{226}(L_c)^2 \frac{\sigma}{\sigma_0} \tag{1-5}$$

Where L_c is characteristic length which is the pore-throat diameter corresponding to the threshold pressure P_t; σ is the rock conductivity at characteristic length; σ_0 is the conductance of brine in the pore space.

MIP data are used to obtain characteristic length and if the electric properties of the fluid used (mercury here) and the rock are known then we can calculate the permeability according to Eq. (1-5). However, the following equation also developed by Katz and Thompson [42, 43] could be used to predict permeability using MIP data only (KT method),

$$k = \frac{1}{89}(L_{max})^2 (\frac{L_{max}}{L_c}) \emptyset S(L_{max}) \tag{1-6}$$

Where L_{max} is the pore-throat diameter at which hydraulic conductance is maximum; L_c is characteristic length; Φ is porosity; S (L_{max}) is calculated as the ratio of V_{Lmax}/V_t .

As pressure is increased, mercury is forced to enter smaller pores. At a critical pressure the mercury spans the sample. The pore-throat diameter corresponding to this critical pressure (threshold pressure P_t) is defined as L_c which is a unique transport length scale and dominates the magnitude of the permeability. The threshold pressure P_t is determined at the inflection point of the cumulative intrusion curve. Webb [87] described in detail the KT method (Eq. (1-6)) for predicting permeability.

Kolodzie [44] published a new equation for estimating permeability of sandstones,

$$Log\, r_{35} = 0.732 + 0.588 Log\, k_{air} - 0.864 Log \emptyset \qquad (1\text{-}7)$$

Where r_{35} is the pore-throat radius (in microns) corresponding to the pressure at which 35% of total pore volume is filled with mercury; k_{air} is the uncorrected air permeability (mD); Φ is porosity (%).

This relationship shows that the permeability of sandstones depends on the r_{35} and the porosity. Compared with Katz and Thompson method, Eq. (1-7) is quite simple. Rezaee et al. [69] summarized the existing similar equations and they used regression analysis to obtain several relationships between permeability, porosity and pore-throat sizes at different mercury saturation percentiles for carbonates and concluded that the median pore-throat radius yields the best correlation coefficient.

1.3 Organization of the Dissertation

This dissertation is concentrated on the application of spontaneous imbibition and mercury intrusion porosimetry in pore structure characterization. The first portion (Chapter 2) of the dissertation proposes a new approach to measuring the effective permeability of building materials by using spontaneous water imbibition. The second portion of the dissertation (Chapters 3-4) describes the derivation process of permeability and gas diffusivity of porous media using MIP data. The third portion of the dissertation (Chapters 5-6) discusses the imbibition behaviors of different reservoir rocks and provides the pore-throat size distribution as well as other pore structure information obtained from MIP to investigate the effect of pore structure on fluid migration within porous media. Specifically, Chapter 5 shows the directional dependency of Barnett shale during spontaneous imbibition because of its layered characteristic and uses this phenomenon to qualitatively identify the wettability information. Also low pore connectivity of Barnett shale is discussed based on the imbibition and MIP results in Chapter 5. Chapter 6 compares the imbibition behaviors of different reservoir rocks and investigates the effect of median pore-throat diameter (D_{50}) on spontaneous imbibition. Finally, a general summary of conclusions and future research will be presented in Chapter 7.

Chapter 2

Using Spontaneous Water Imbibition to Measure the Effective Permeability of Building Materials

2.1 Abstract

The purpose of the present work is to introduce a new approach to measuring the effective permeability of building materials by using spontaneous water imbibition. A new linear relationship between water imbibition rate and the reciprocal of air recovery is derived and used as the basic theory to obtain the permeability information. The impact of buoyant-force change on the imbibition results is taken into consideration, which makes our results more accurate and reliable. The calculated effective permeabilities of three building materials, including limestone, concrete, and brick, are reasonably compared with permeability data in the literature.

2.2 Introduction

Permeability is an important index of the durability of building materials. Several approaches to measuring the permeability of building materials have been proposed. For example, critical voltage of concrete at limited currents is used to evaluate the concrete permeability [53]. Also the permeability of concrete can be obtained by the conductivity of concrete when saturated with concentrated salt according to the Nernst-Einstein equation [52].

Spontaneous imbibition is the process during which the non-wetting fluid (air) in a porous medium is displaced by a wetting fluid (water) due to capillary forces. Li and Horne [48] calculated the capillary pressure and effective permeability from spontaneous water imbibition data for sandstones. However, this work is the first time the effective permeability of building materials has been obtained from spontaneous imbibition.

2.3 Theory

Based on Darcy's law and several assumptions, Li and Horne [48] derived the following four equations,

$$Q_w = \frac{dN_{wt}}{dt} = a\frac{1}{\eta} - b \qquad (2\text{-}1)$$

where:

$$a = \frac{Ak_w(S_{wf} - S_{wi})}{\mu_w L} P_c \qquad (2\text{-}2)$$

$$b = \frac{Ak_w}{\mu_w} \Delta\rho g \qquad (2\text{-}3)$$

$$\eta = \frac{N_{wt}}{V_p} \qquad (2\text{-}4)$$

where Q_w is the water imbibition rate; N_{wt} is the volume of water imbibed into the sample; t is imbibition time; η is the air recovery by water imbibition in terms of pore volume; A is the cross-section area of the sample; k_w is the effective permeability of water phase at a water saturation of wetting front S_{wf} ; S_{wi} is the initial water saturation in the sample; P_c is the capillary pressure at S_{wf}; μ_w is the viscosity of water; L is the sample length; $\Delta\rho$ is the density difference between water and air; g is the acceleration due to gravity; V_p is the pore volume of the sample.

According to Eq. (2-3), Li and Horne [48] obtained the effective water permeability at the water saturation of S_{wf} as follows:

$$k_w = \frac{\mu_w}{A\Delta\rho g} b \qquad (2\text{-}5)$$

In this study, the derivation process is similar to the studies of Li and Horne [48], but with a little difference. They used the following equation as one of their basic equations:

$$v_w = -\frac{k_w}{\mu_w}(\frac{\partial p_w}{\partial x} + \rho_w g) \tag{2-6}$$

where v_w is the flowing velocity of water phase; p_w is the pressure of water phase at the position x; ρ_w is the water density.

However, use of '+' sign inside the parenthesis in Eq. (2-6) is disputable. Hassanizadeh [36] used Eq. (2-7) to describe the Darcy velocity for wetting phase in the research on the physics of two-phase flow. Considering simultaneous flow of two incompressible and immiscible fluid phases (water and oil) inside a porous medium, Hilfer [38] presented the same equation as Eq. (2-7). Silin et al. [78] conducted a research on vertical gas plume migration through a heterogeneous porous medium, which was similar to our imbibition experiments. In their research, they assumed that the carbon dioxide plume crossed a thick aquifer with uniform flow properties. According to their assumption on the vertical direction, a positive Darcy velocity means upward flow. Then they derived the same relationships between the Darcy velocities of gas and brine and their respective pressure gradients with Eq. (2-7) according to Darcy's law for two-phase flow.

$$v_w = -\frac{k_w}{\mu_w}(\frac{\partial p_w}{\partial x} - \rho_w g) \tag{2-7}$$

As a result, a new equation is derived to replace Eq. (2-1):

$$Q_w = \frac{dN_{wt}}{dt} = a\frac{1}{\eta} + b \tag{2-8}$$

where,

$$b = \frac{Ak_w}{\mu_w}\rho_s g \tag{2-9}$$

ρ_s denotes the sum of water and air densities. If we plot the water imbibition rate (Q_w) versus the reciprocal of air recovery ($1/\eta$), the intercept on the axis of water imbibition rate (b value) will be a positive value according to Eq. (2-8). We can then derive the equation of k_w from Eq. (2-9) as follows,

$$k_w = \frac{\mu_w}{A\rho_s g} b \tag{2-10}$$

This equation is used in this work to obtain the effective permeability k_w.

2.4 Materials and Experimental Procedure

The following three types of building materials were used in this study: concrete, limestone and red brick. All samples were cut into rectangular prisms and given a unique name. The properties and sources of these building materials are listed in Table 2-1.

Table 2-1 Sample Properties and Sources

Sample ID	Length (cm)	Width (cm)	Height (cm)	Porosity[a] (%)	Source[b]
Concrete 1	1.575	1.524	6.777	20.0	Home Depot
Concrete 2	1.766	1.713	1.579	19.7	Home Depot
Limestone	3.225	2.878	5.221	15.3	Cathedral Stone Products, Hanover Park, Maryland
Red brick	2.778	2.931	2.425	20.3	Triangle Brick Company, Durham, North Carolina

[a] Porosity was determined by using vacuum saturation method [70].
[b] From Sang Don Lee (USEPA, personal communication).

After completing the porosity measurements, all sides (except top and bottom faces) of each sample were covered with quick-cure epoxy to avoid the water evaporation from the side surface of the samples during imbibition experiments. Each sample was oven-dried at 60 °C for at least 48 hours and then cooled to room temperature (22.5±0.5 °C) in a desiccator. During the imbibition experiment, the sample was suspended by a sample holder that was connected to a bottom-weighing electronic balance by a hook. A simplified schematic of the apparatus for imbibition test is shown in Figure 2-1. The sample was located inside an imbibition chamber with a water reservoir (a glass Petri dish) on its floor. Additional beakers of water were placed inside the chamber to keep the humidity inside the chamber constant at above 98%. The chamber position was vertically adjusted by a support jack below the chamber to make the sample submerged in water to about 1 mm depth to start the imbibition test. The balance automatically recorded the sample weight as frequently as once per second [39]. The imbibition tests were stopped by lowering the support jack and weighing the sampling weight after using a moist tissue to wipe off the excess water at the sample bottom. Imbibition experiments were repeated at least three times on the same sample for different experimental duration.

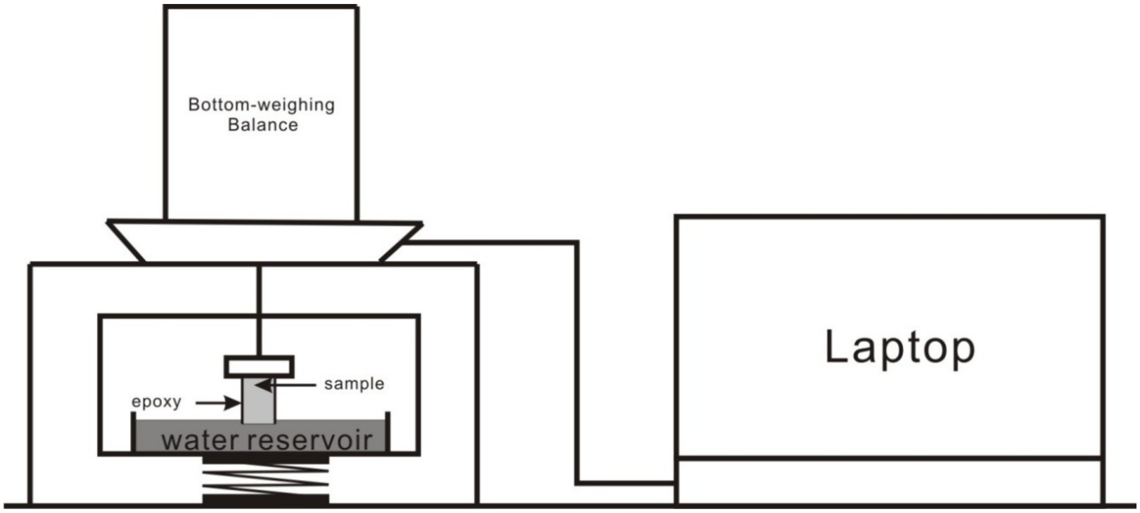

Figure 2-1 Schematic of the Apparatus for Imbibition Test

2.5 Results and Discussion

2.5.1. Water Imbibition vs. Time

We measured the water imbibition behavior of each building material sample. A typical imbibition curve is shown in Figure 2-2 for limestone. The artificial weight gain produced by the buoyant-force change, which was caused by imbibition and evaporative losses, was corrected [39]. The check weight, obtained directly by weighing the sample with sample holder before and after each imbibition experiment, is consistent with the ultimate cumulative imbibition amount corrected by considering both evaporation and imbibition correction for the buoyant-force change (Figure 2-2). It can be seen from Figure 2-2 that the amount of water imbibed into the limestone sample reached the maximum value at about 250 min and the water imbibition rate became quite low after that time.

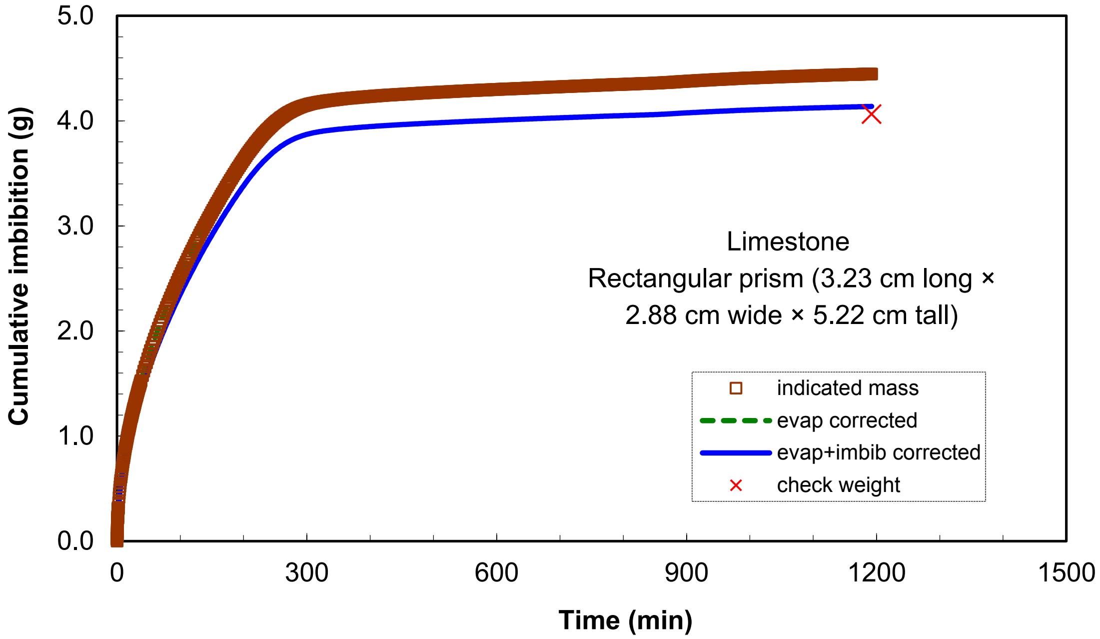

Figure 2-2 Water Imbibition into the Limestone Sample (Data for indicated mass from direct balance reading overlaps with these after evaporation correction because of the small evaporation amount.)

2.5.2. Water Imbibition Rate vs. the Reciprocal of the Air Recovery

Figure 2-3 shows that a linear relationship exists between the water imbibition rate and the reciprocal of the air recovery by water imbibition, and this linear relationship corresponds to the fast imbibition part (less than 250 min) shown in Figure 2-2. The intercept (*b* value) on the axis of water imbibition rate is positive, which is consistent with Eq. (2-8) and the definition of *b* and proves that the use of Eq. (2-7) is appropriate in this work. The effective permeability can then be obtained from Eq. (2-10) and the results are listed in Table 2-2. The water saturation immediately behind the wetting front (i.e., effective porosity) ranges from 55-99% for these building materials. The k_w values, at the corresponding wetting front saturation, are similar to the reported absolute permeability (k) of $(6–39)\times10^{-15}$ m^2 for brick [8], $(2–27)\times10^{-15}$ m^2 for limestone [10] and $(10^{-2}-10^{2})\times10^{-15}$ m^2 for concrete [66]. Note that we are not aware of unsaturated effective permeability for these building materials, and even the absolute permeability values are very limited in the literature.

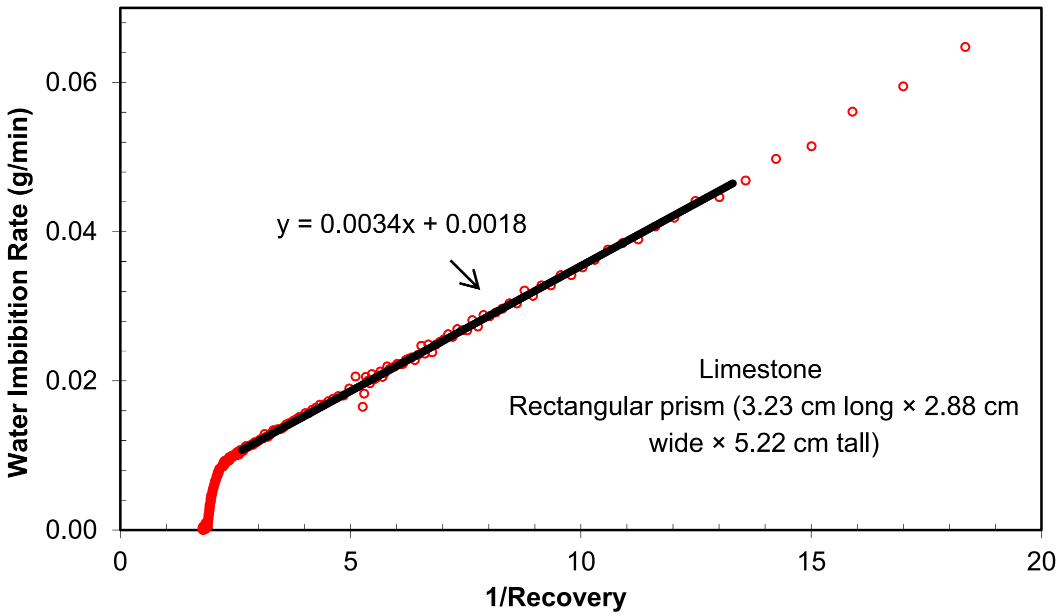

Figure 2-3 Water Imbibition Rate vs. the Reciprocal of the Air Recovery

Table 2-2 Result of Effective Permeability from Spontaneous Imbibition Data

Sample ID	A (cm^2)	b^a (cm^3/min)	S_{wf}^a	$k_w^{a,b}$ (md)	k from references (md)
Concrete 1	2.400	0.0011±0.0006	0.99±0.06	8.07±4.17	10^{-2}-$10^{2\ c}$
Concrete 2	3.025	0.0017±0.0004	0.80±0.06	9.60±2.46	10^{-2}-$10^{2\ c}$
Limestone	9.282	0.0026±0.0008	0.55±0.01	4.85±1.48	2–27^d
Red brick	8.142	0.0311±0.0072	0.73±0.08	65.2±15.0	6–39^e
ρ_g (at 20 °C) = 1.2 kg/m^3; ρ_w(at 20°C) = 998.2 kg/m^3; g = 9.8 m/s^2; μ_w (at 20 °C) = 1.002 (N·S/m^2)×10^{-3}.					

[a] Average ± standard deviation for at least three replicate measurements.

[b] Caculated according to Eq. (2-10).

[c] From Picandet et al. [66].

[d] From Boving and Grathwohl [10].

[e] From Bentz et al. [8].

2.5.3. Discussion

The standard deviation for k_w shown in Table 2-2 is somewhat high and there are several possible factors to cause it. The initial state of the same sample may be slightly different in each imbibition experiment although we tried to minimize this effect by treating samples similarly before and after each run. The permeability of the building materials used here is relatively low which can also contribute to the fluctuations among permeability values for the same sample. The most possible factor is from the micro-scale sample heterogeneity, which is very sensitively reflected in the measured unsaturated effective permeability.

We did not obtain the permeability of asphalt concrete by using the same method and one possible reason is the low porosity (2.2%) and the poor connectivity; this will be investigated in the future work.

2.6 Conclusion

A new approach has been developed here to measure the effective permeability of unsaturated building materials from simple imbibition tests. The new derived linear relationship between water imbibition rate and the reciprocal of air recovery is corroborated by the results of imbibition experiments. The values we got here for permeability are in line with literature permeability results by using different approaches (e.g., mercury injection porosimetry). Considering the low permeability of these building materials and the factors mentioned above, the standard deviations for k_w are acceptable. This new method can be applied to materials with a relatively high porosity (e.g., >15% as tested in three materials in this work) and well-connected pore structure.

Chapter 3

Estimating Permeability Using Median Pore-throat Radius Obtained from Mercury Intrusion Porosimetry

3.1 Abstract

Mercury intrusion porosimetry (MIP) has been widely used to characterize the pore structure for various types of porous media. Several relationships between permeability and pore structure information (e.g., porosity and pore-size distribution) have been developed in the literature. The focus of this work is to introduce a new, and simpler, empirical equation to predict permeability by solely using the median pore-throat radius (r_{50}), which is the pore-throat radius corresponding to the 50% mercury saturation. The total of 18 samples used in this work has a wide range of permeability, from 10^{-6} to 10^{3} mD, which makes the new equation more applicable. The predicted permeabilities by using the new equation are comparable with permeability values obtained from other measurement methods, as shown from ten samples with permeability data measured with nitrogen.

3.2 Introduction

Permeability is an important parameter to characterize the ease with which a porous medium transmits fluids, and an accurate measurement or estimation of permeability has been a challenging task, especially for media with low permeability. Due to the limitations (e.g., required experimental apparatus and long measurement duration, especially for tight samples) associated with the permeability measurement, several empirical relationships have been published to predict permeability based on other parameter(s) that are relatively easier to obtain; but most of these relationships involve more than one parameter variable. As one of the first empirical relationships, Hazen [37] derived a simple equation to calculate hydraulic conductivity of unconsolidated porous materials by only using effective grain size. The recent work of Rezaee et al. [69] concluded that the median pore-throat radius yields the best correlation coefficient for permeability, porosity and pore-throat size of carbonate rocks.

Over the past 30 years, mercury intrusion porosimetry (MIP) has become a well-established technique for characterizing porous media, since Washburn [86] proposed the relationship between capillary pressure and the pore radius as the basic theory for MIP [29]. Compared with other pore size characterization approaches (e.g. gas sorption), MIP is based on a simple principle and could cover a wide range of pore sizes (from about 3 nm to 300 μm for current models of MIP instruments), which makes it a powerful characterization tool. In addition, MIP measurement is less time-consuming, one MIP test is usually completed within 1 hour for not-so-tight samples like sandstones and carbonates, while for tight samples (e.g., shales) it usually needs 2 hours because of long evacuation time due to its nano-sized pores during low pressure analysis. Because of the extremely low permeability, which is usually in nano darcy, it is expensive to measure the permeability of shale samples directly. As a result, estimating permeability of shale samples by MIP could be an alternative method.

Derivation of permeability from MIP data has been pursued by several researchers [42, 43, 82], among them the Katz and Thompson [42, 43] method (called KT method in this paper) is the one we use to calculate permeability and our new equation is derived based on these calculated values. The validation of the KT method will be provided in section 3.6.2 of this paper. We will also compare the permeability values measured by N_2 with permeability calculated by using our new equation and the equation proposed by Rezaee et al. [69].

3.3 MIP Background

As a non-wetting fluid for most porous media, mercury will not invade pores unless an external pressure is applied. The diameter of the pores invaded by mercury is inversely proportional to the applied pressure; the higher pressure is applied, the smaller pores invaded by mercury. Washburn [86] developed the following equation based on the assumption that all the pores are cylindrical in shape,

$$\Delta P = -\frac{2\gamma cos\theta}{R} \tag{3-1}$$

where ΔP is the pressure difference across the curved mercury interface; γ is the surface tension of mercury; θ is the contact angle between mercury and the porous medium; and R is the corresponding pore-throat radius. Using γ = 485 dynes/cm and θ = 130°, Eq. (3-1) becomes

$$\Delta P = \frac{90.43}{R} \tag{3-2}$$

where ΔP is in psia and R is in micrometers (µm).

During the sample analysis, MIP collects the data of applied pressure and cumulative intrusion volume at that specific pressure. Katz and Thompson [42, 43] introduced the following equation to calculate permeability based on the MIP data:

$$k = \frac{1}{89}(L_{max})^2(L_{max}/L_c)\phi S(L_{max}) \tag{3-3}$$

where k (darcy) is air permeability; L_{max} (µm) is the pore-throat diameter at which hydraulic conductance is maximum; L_c (µm) is the characteristic length which is the pore-throat diameter corresponding to the threshold pressure P_t (psia); ϕ is porosity; $S(L_{max})$ represents the fraction of connected pore space composed of pore width of size L_{max} and larger.

The threshold pressure P_t is determined at the inflection point of the cumulative intrusion curve and the selection of L_{max} is dependent on P_t. Webb [87] described in detail the KT method (Eq. (3-3)) for predicting permeability, and the step-by-step data processing procedures to determine each parameter in Eq. (3-3) will be shown in section 3.5.

3.4 Materials and Experimental Procedure

In order to obtain a representative empirical relationship to predict permeability, a total of 18 samples with a wide range of permeability were tested by MIP method; the samples are listed in Table 3-1. Each sample (mostly cube-sized, with the largest linear dimension of about 1.5 cm) was oven-dried at 60 °C for at least 48 hours to remove moisture in pore spaces and then cooled to room temperature (~23ºC) in a desiccator before the MIP test.

During an MIP test, each sample underwent two analyses: low-pressure and high-pressure analyses. The highest pressure produced by Micromeritics AutoPore IV 9510 (Norcross, GA) is 60,000 psia (413MPa), and the pore-throat diameter corresponding to this pressure according to Eq. (3-2) is about 3.0 nm. The largest pore-throat diameter recorded by MIP is about 300 microns under low-pressure analysis. The samples were evacuated to 50 μmHg (i.e. 0.05 Torr or 6.7 Pa). Equilibration time (the minimum time duration to achieve a stable mercury level before moving on to the next pressure value) was chosen to be 50 s.

Among these samples, ten of them were measured for permeability to nitrogen gas ($k_{measure}$ in Table 3-2), using rock cylindrical core samples (2.54 cm i.d., 4 cm height), by Core Laboratories Inc. (Aurora, CO or Houston, TX) following standard methods in API RP 40 [3].

Table 3-1 18 Samples Tested by MIP

1	Asphalt	6	Dolomite	11	Barnett Shale 1[a]	16	Yucca Mt. Tuff
2	Red brick	7	Gray Chalk	12	Barnett Shale 2	17	Hanford Basalt
3	Concrete	8	White Chalk	13	Barnett Shale 3	18	Costa Rica Basalt
4	Granite	9	Berea Sandstone	14	Barnett Shale 4		
5	Limestone	10	Indiana Sandstone	15	Japan Mudstone		

[a] Barnett shale sample 1-4 come from different depths (7109 ft,7169 ft, 7199 ft,7219 ft) in the same well.

3.5 Data Analysis of MIP Tests

Besides permeability, several other pieces of useful information could be derived from MIP data, like bulk density, porosity and tortuosity [33]. In order to concentrate on the purpose of this study, we will only introduce the data-processing procedures related to permeability calculation. The KT method is the basic theory we use here to calculate the permeability and to derive our new equation. Although Webb [87] has described KT method in detail, it is still necessary to present this process clearly by giving an actual example calculation.

Here we discuss the permeability calculation process of sample 8 (white chalk) in Table 3-1, which is a type of carbonate. After obtaining the raw data of MIP test (as shown in Figure 3-1), the first and important step is to define the threshold pressure P_t, which is determined at the inflection point of the cumulative intrusion curve. This inflection point (414.6 psia) is defined as the highest point in the log differential intrusion curve, which is shown in Figure 3-2. The characteristic length L_c corresponding to P_t can be calculated as 0.436 μm according to Eq. (3-2), and V_t can be obtained directly from the cumulative intrusion curve, which is 0.0875 mL/g.

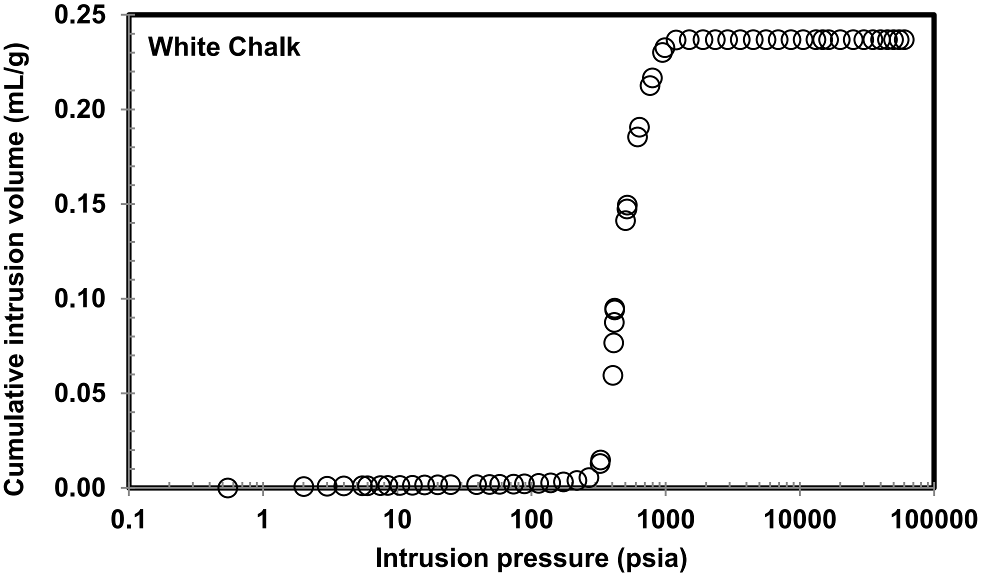

Figure 3-1 Cumulative Intrusion Volume vs. Intrusion Pressure for White Chalk

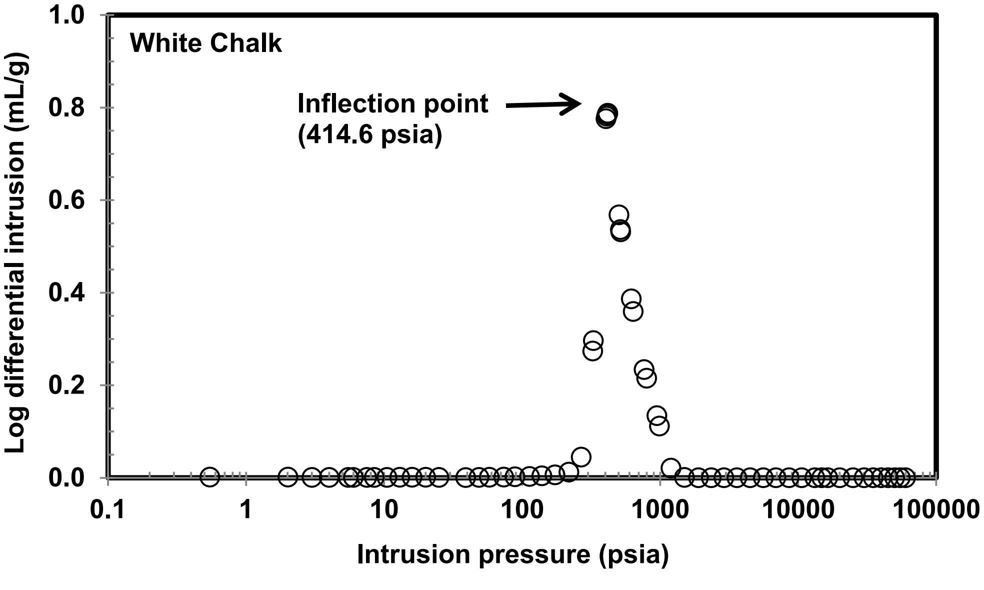

Figure 3-2 Log Differential Intrusion vs. Intrusion Pressure for White Chalk

The next step is to obtain L_{max} and V_{Lmax}. V_t is subtracted from each cumulative intrusion volume V_c at each pressure in the dataset from P_t to the maximum pressure. Then the net volume (V_c-V_t) times the diameter-cubed for the corresponding pressure is plotted as a function of pore-throat diameter. As shown in Figure 3-3, the pore-throat diameter of 0.349 μm corresponding to the maximum y-value is L_{max} and the cumulative intrusion volume corresponding to this diameter is denoted as V_{Lmax}, which is 0.149 mL/g. The total intrusion volume (V_{tot}) for the sample of white chalk is 0.237 mL/g. According to the definition of $S(L_{max})$, (V_{Lmax}) /(V_{tot}) can be calculated as 0.629.

The porosity (ϕ) of white chalk is 0.346, which can be directly obtained from MIP measurement. Until now all the required parameters in Eq. (3-3) are known, and we can calculate the permeability of white chalk to be 0.239 mD. All the other samples were processed to obtain the permeability by the same procedures described above.

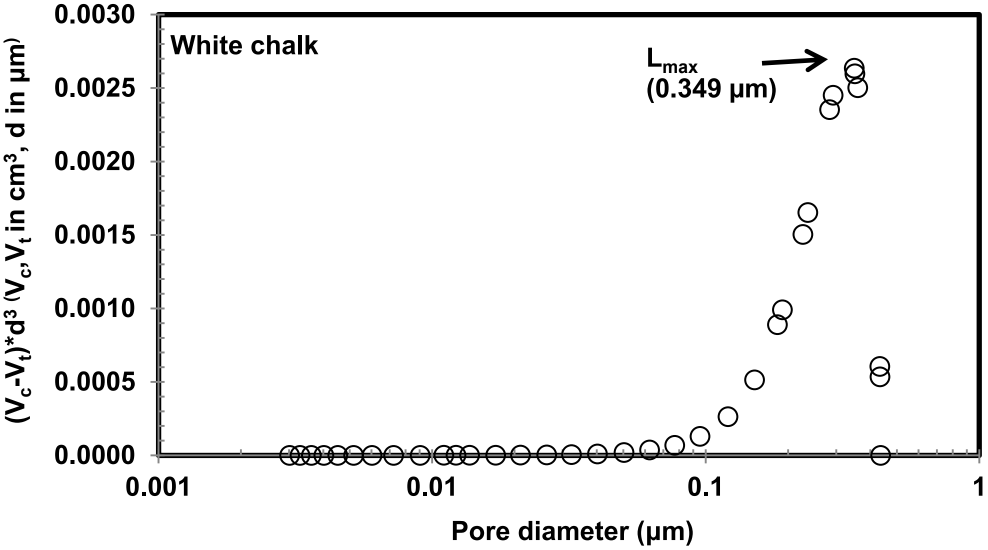

Figure 3-3 Determination of L_{max} in White Chalk

3.6 Results

3.6.1. Reproducibility of MIP Tests

We perform triplicate MIP measurements on Berea sandstone and Barnett Shale no. 3 to evaluate the repeatability of MIP. Ideally, a repeatability test should be carried out on the same piece of sample. However, this is not possible in the case of MIP test because the sample is contaminated with mercury after MIP test. As a result, we choose three representative samples from the same rock block to check the repeatability of MIP. For Berea sandstone, we obtain the porosity as 22.86 ± 1.72% and r_{50} as 11.89 ± 0.44 µm; for Barnett Shale no. 3, the porosity is 5.29 ± 0.59% and r_{50} is 0.0031 ± 0.0002 µm. Considering the inherent heterogeneity of natural rock, this result is acceptable and the repeatability of MIP is verified.

3.6.2. Comparison between k_{cal} and $k_{measure}$ (Permeability Measured by N_2)

Using regression analyses, Rezaee et al. [69] obtained a set of relationships between permeability, porosity and pore-throat size for 144 carbonate samples. They found that the following equation has the highest correlation coefficient between measured and calculated permeability,

$$Log\ k = -1.160 + 1.780\ Log\ \phi + 0.930\ Log\ r_{50} \tag{3-4}$$

where k is the air permeability (mD); ϕ is porosity (%); r_{50} is the median pore-throat radius corresponding to 50% mercury saturation (µm).

The new empirical equation (Gao-Hu equation in this paper), by plotting log k_{cal} (permeability calculated by using KT method) versus log r_{50} (as shown in Figure 3-4), is obtained as follows,

$$Log\ k = 2.225 Log\ r_{50} + 0.214 \tag{3-5}$$

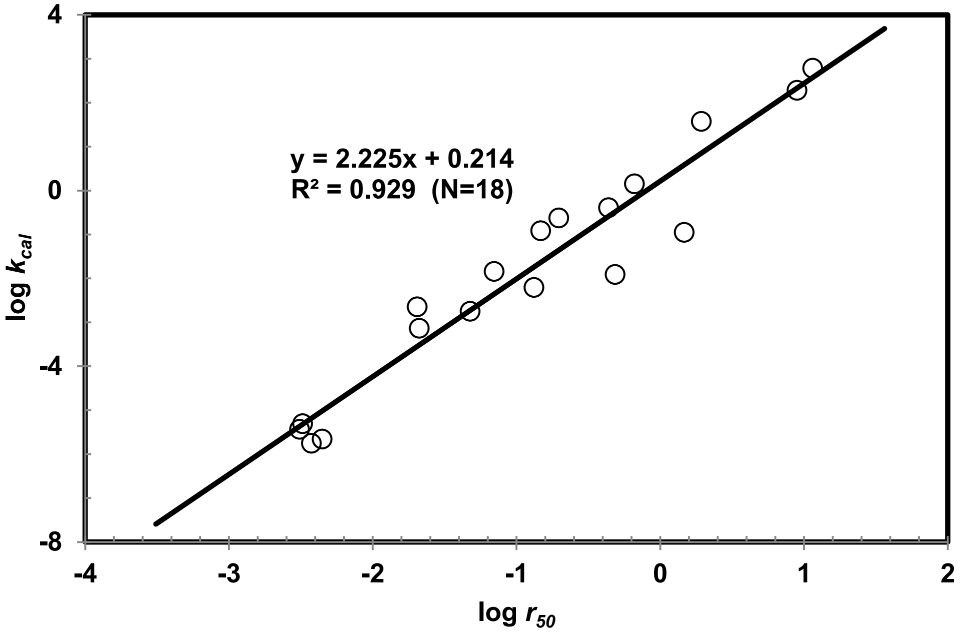

Figure 3-4 Log k_{cal} versus Log r_{50} for all 18 Samples in Table 3-1

Together with k_{cal} and $k_{measure}$, median pore-throat radii (r_{50}) of ten samples which can be directly obtained from cumulative intrusion curve are listed in Table 3-2. Apart from two building materials (concrete and red bick), there is only a slight difference between k_{cal} and $k_{measure}$ for all other natural rocks. This is encouraging, considering the difficulty of permeability measurement, for difference within1-2 orders of magnitude obtained by different approaches for the same sample is not uncommon. As a result, the KT method is reliable to calculate permeability and selection of k_{cal} as the sample permeability to derive the new equation is appropriate.

We also plot $k_{measure}$ versus log r_{50}, and the fitted equation and the R^2 value are shown in Figure 3-5. Although the R^2 value is not high (0.723), it indeed indicates a relationship exists between permeability and r_{50}.

Table 3-2 Comparison between k_{cal} and $k_{measure}$

Sample ID	Sample name	Porosity	r_{50} (µm)	k_{cal} (mD)[a]	$k_{measure}$ (mD)[b]	$k_{measure}/k_{cal}$
2	Red brick	0.212	0.662	1.42E+00	30.7	21.54
3	Concrete	0.208	0.070	1.45E-02	0.151	10.44
4	Granite	0.011	0.485	1.24E-02	0.003	0.24
5	Limestone	0.145	1.930	3.78E+01	18.3	0.48
6	Dolomite	0.091	0.436	4.09E-01	9.8E-02	0.24
7	Gray Chalk	0.320	0.147	1.22E-01	3.2E-01	2.63
8	White Chalk	0.346	0.197	2.40E-01	4.3E-01	1.80
9	Berea Sandstone	0.248	11.491	6.13E+02	9.1E+02	1.48
10	Indiana Sandstone	0.167	8.945	1.92E+02	1.8E+02	0.94
16	Yucca Mt. Tuff	0.096	0.021	7.33E-04	2.0E-04	0.27

[a] k_{cal}: permeability calculated by using KT method;
[b] $k_{measure}$:permeability measured by N_2 (Klinkenberg effect has been taken into account).

3.6.3. Comparison between Gao-Hu Equation and Rezaee Equation

We derive a linear relationship between log k_{cal} and log r_{50}, which is called the Gao–Hu equation in this paper. The comparison between Gao-Hu and Rezaee equations is shown in Figure 3-6, where k_{cal} is used as the sample permeability to compare the utility of these two equations. The permeability calculated using the Gao–Hu equation exhibits a better agreement than the Rezaee equation. All the permeability values calculated using the Gao–Hu equation are closely distributed along the y = x line in Figure 3-6, while the permeabilities calculated using Rezaee equation deviate somewhat from the y = x line and this phenomenon becomes more obvious for samples with a low permeability. Rezaee et al. [69] pointed out that their equation has a good outcome when it is applied to carbonates and we can arrive at the same conclusion from Figure 3-6 in which carbonates have been differentiated from other samples by using different symbols. As a result, both the Gao–Hu equation and the Rezaee equation are applicable to carbonates, while the Rezaee equation becomes less valid when dealing with tight samples like shale compared with the Gao–Hu equation.

In order to draw a more reliable conclusion, we compare the $k_{measure}$ with permeability calculated by the Gao–Hu equation and the Rezaee equation for eight natural rocks; the results are shown in Figure 3-7. We add trend lines to each group of permeabilities, and the equations of the trend lines and the R^2 values together with the number of samples (N) are given in Figure 3-7. Again, the permeability values calculated using the Gao–Hu equation are closely distributed along the y = x line, which verifies the validity of the Gao–Hu equation.

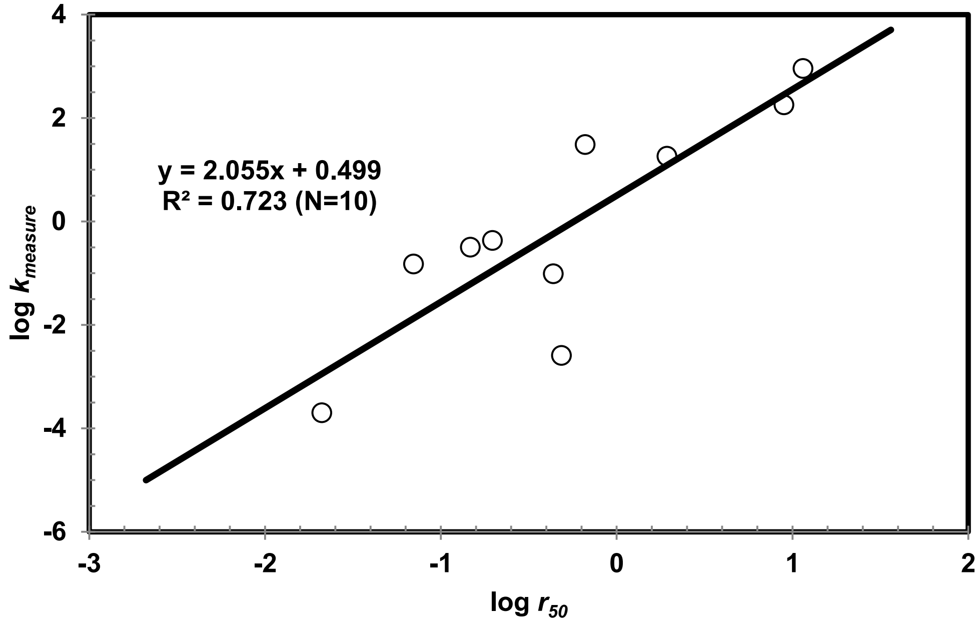

Figure 3-5 Log $k_{measure}$ versus Log r_{50} for Ten Samples in Table 3-2

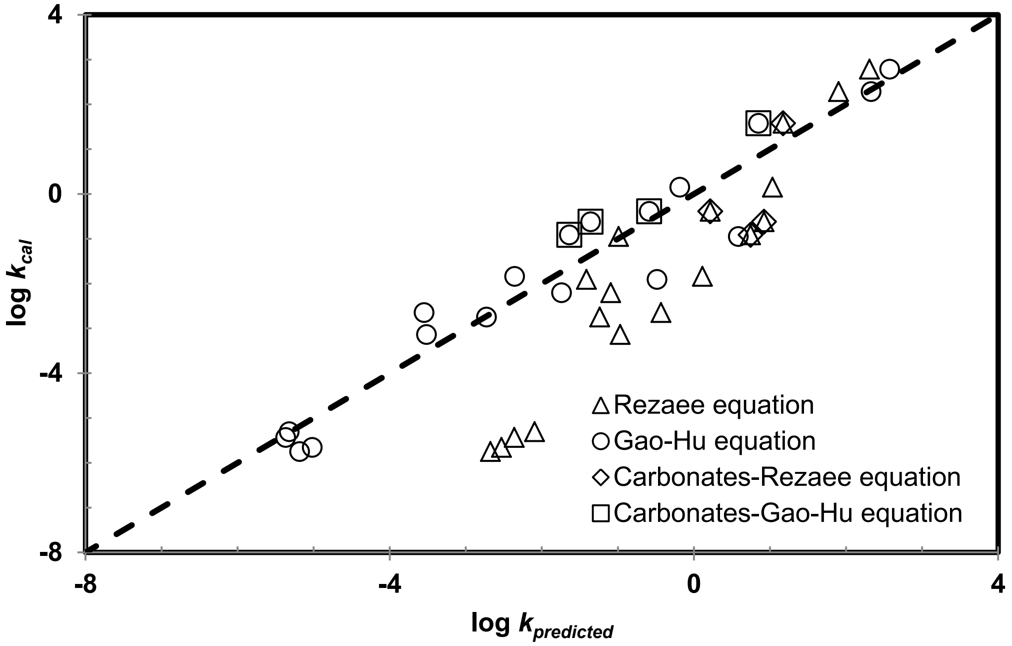

Figure 3-6 Comparison between Log k_{cal} and Log $k_{predicted}$ ($k_{predicted}$ stands for predicted permeability using Gao–Hu equation or Rezaee equation)

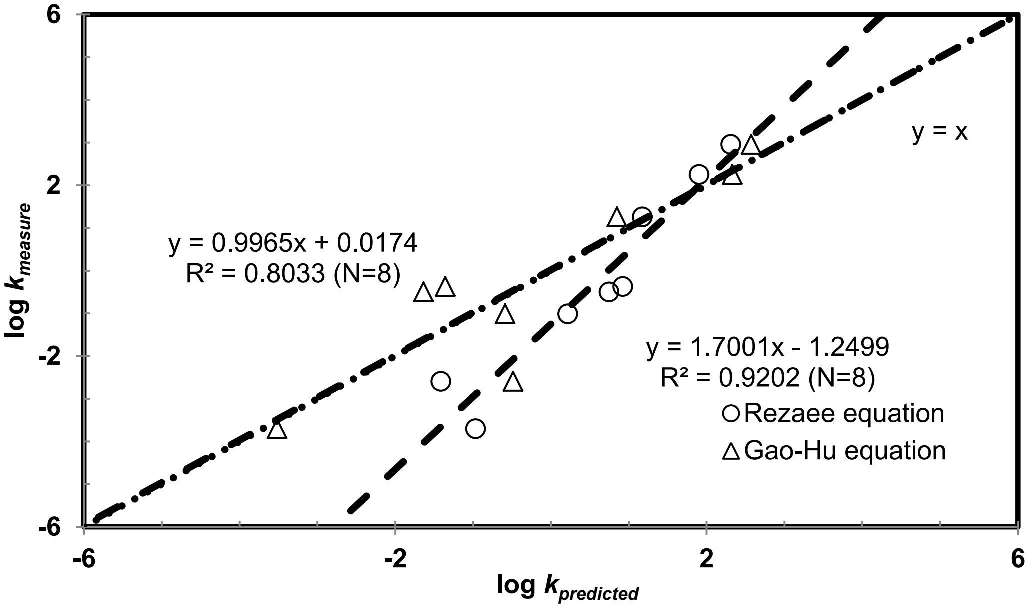

Figure 3-7 Comparison between Log $k_{measure}$ and Log $k_{predicted}$

3.7 Conclusion

This study presents a new equation which solely uses the median pore-throat radius to estimate the permeability of porous consolidated media. Compared with the existing relationships such as Rezaee equation, the advantages of our new equation include the simple form, high reliability and wide applicability. Nowadays, more and more unconventional reservoirs with relatively low permeability are investigated and explored, which makes the new equation have a more realistic meaning. Our results also show that the KT method is reliable to obtain permeability from MIP data, from the good agreement with the measured permeability using N_2.

The reason that porosity could be ignored in our new equation may be that the effect of porosity on permeability is negligible, compared with the effect of median pore-throat radius. The sole use of median pore-throat radius to predict permeability indicates that r_{50} may control the fluid flow in porous media.

For consolidated porous materials (rocks) this work is the first to only relate permeability to median pore-throat radius without considering other parameters. The samples we use here also have a wide range of permeability, from sandstone ($\sim 10^3$ mD) to shale ($\sim 10^{-6}$ mD), which makes the new method more applicable.

Although MIP has been developed for a long time, there are still some issues related to its application [20, 23]. Hysteresis phenomenon (nonreversibility between mercury intrusion and extrusion curves) and different contact angles between mercury and different porous media have attracted a lot of researchers' attention [60, 92]. In this paper, we used the median pore-throat radius from the mercury intrusion curve; the new equation may be improved as more data with rocks are collected in the future.

Chapter 4

Gas Diffusivity in Porous Media: Determination by Mercury Intrusion Porosimetry and Correlation to Porosity and Permeability

4.1 Abstract

Much effort has been extended on diffusivity measurement because diffusion can dominate mass transport in porous media of low hydraulic conductivity. The main purpose of this work is to derive the gas diffusivities of building materials, rocks and sediments using the average pore size measured by mercury intrusion porosimetry (MIP). MIP has been utilized for decades to obtain the pore-size distribution of porous media. We performed triplicate MIP tests on concrete and Berea sandstone to evaluate the repeatability of MIP data. Gas diffusivity results are consistent with literature data using the gas diffusion methods. Our results show that the relationship between gas diffusivity and porosity is analogous to Archie’s law and that two groups of rocks are differentiated according to the cementation factor m value in an Archie’s-type relationship. It also appears that gas diffusivity exhibits an increasing trend with an increase of permeability, and two different exponential relationships exist between permeability and porosity for these two groups of rocks.

4.2 Introduction

Diffusion and advection are two important processes controlling mass transport in porous media. The relative contribution of these two processes depends primarily on the properties of the porous medium. For example, Gillham et al. [30] pointed out that diffusion dominates mass transport when seepage velocity is on the order of 0.005 m/year, which is higher than that of many rocks. Generally, diffusion may be the dominant transport process in porous media with very low permeability [10]. As a result, a comprehensive understanding of diffusion processes in porous media becomes essential for waste disposal, carbon dioxide storage, evaluation of building materials, and gas production from unconventional reservoirs [12, 16, 74, 75].

The measurement of diffusivity could be achieved by using liquid-phase or gas-phase tracers. Shackelford [75] reviewed the methods used to measure effective diffusion coefficients of chemical species and summarized the advantages and disadvantages of each method. The diffusion chamber method has been used to make gas diffusivity measurements in unconsolidated [72] and consolidated media [65].

Mu et al. [64] indicated that the effective diffusion coefficient is strongly dependent on pore size when the average pore size is less than 1 μm, which is the situation for many rocks. As an advanced tool in characterizing pore size distribution, mercury intrusion porosimetry (MIP) could provide useful information on pore structure (such as porosity and average pore size). Compared with traditional methods (e.g., the gas diffusion approach), determination of gas diffusivity from the pore-size information obtained through MIP is less time-consuming (usually requiring less than two hours), and MIP covers a wide range of pore sizes (from 10^{-4} to 10^{-9} m), making it more convenient and applicable. Using MIP, Seo et al. [74] evaluated the effective diffusion coefficient in building materials and absorbents, and presented the effective diffusion coefficients of different gases for these materials. In this work we investigate the effective gas diffusion coefficients in different types of rocks (sedimentary and igneous) and unconsolidated sediments with different grain sizes, and in building materials. In addition, we explore the correlation of gas diffusivity to porosity and permeability.

4.3 Materials

Three types of porous media (listed in Table 4-1) were used in our research. They included two building materials, eight rocks, and four unconsolidated sediments with different grain sizes. All the consolidated samples were reduced to small pieces (>5 mm but < 15 mm) according to the dimension of the cylindrical bowl of a penetrometer, which is the sample container by MIP. Sediments were collected from the vadose zone (~3-4 m below ground surface) of the Integrated Field-Scale Research Challenge site at the Hanford 300 Area in Richland WA, and were sieved into four groups of <75 μm, 75-500 μm,500 μm-2 mm and <2 mm [22]. During MIP tests, these unconsolidated samples were placed in a penetrometer specially designed for powder samples.

Table 4-1 Samples Used in This Study

Sample		Source
Building materials	Concrete	Home Depot
	Red brick	Triangle Brick Company, Durham, North Carolina
Rocks	Limestone	Hanover Park, MD
	Dolomite	Unknown
	Indiana sandstone	Gas storage formation, Lombard, IL
	Berea sandstone	Berea Quarry, OH
	Gray chalk	Negev Desert, Israel
	White chalk	Negev Desert, Israel
	Tuff	Yucca Mountain, NV
	Mudstone	Hokkaido, Japan
Unconsolidated sediments	<2 mm	Hanford Site, Richland, WA
	500 μm-2 mm	Hanford Site, Richland, WA
	75-500 μm	Hanford Site, Richland, WA
	<75 μm	Hanford Site, Richland, WA

Before MIP testing, all the samples were oven-dried at 60 °C for at least 48 hours, and were then cooled to room temperature (~22.5ºC) in a desiccator. Porosity, average pore size d_a (defined in Section 4.4.2.2) and median pore size (d_{50}), which is the pore diameter corresponding to 50% mercury saturation, were obtained from the results directly reported by MIP. The calculation of permeability and diffusivity was based on these pore size data, as described in detail in the next Section.

4.4 Gas Diffusivity: Theoretical Background and Measurement by MIP

4.4.1. Definition of Diffusivity

Gas diffusion in porous media is a process caused by the random thermal motion of gas molecules, which can be described by Fick's first law, which takes the form of Eq. (4-1) if the diffusion occurs under steady state conditions in a one-dimensional system at uniform temperature and pressure [10],

$$Fg = -D_e \frac{\partial C}{\partial x} \tag{4-1}$$

where F_g is the diffusive gas flux [M L^{-2} T^{-1}]; D_e is the effective gas diffusion coefficient in the porous medium [L^2 T^{-1}]; C denotes gas concentration in the pore[M L^{-3}]; and x denotes distance [L].

Defined as the ratio of D_e to the gas diffusion coefficient in air, D_a, gas diffusivity (D') is often expressed as an exponential function of porosity [31], in a form analogous to Archie's law,

$$\frac{D_e}{D_a} = D' = \emptyset_a^m \tag{4-2}$$

where $\emptyset_a$ is air-filled porosity and m is an empirical exponent called cementation factor.

The m value in Archie's relationship (Eq. (4-2)) depends on the pore geometry of the porous media and several different m values are reported in the literature [65]. For example, Archie [6] reported m value from 1.8 to 2.0 for consolidated sand, and Adler et al. [1] obtained an m value as 1.64 for Fontainebleau sandstone.

4.4.2. Theoretical Background

4.4.2.1. MIP as a characterization tool

As a well-developed characterization tool, MIP has received attention from many researchers and is commonly applied in pharmacy, civil engineering and reservoir engineering [45, 85, 88].

Because of its non-wetting property to most geological materials, mercury will not invade pores unless it is applied with an external pressure. The diameter of the pores invaded by mercury is inversely proportional to the applied pressure, which is expressed as the following equation developed by Washburn [86], based on the assumption that all pores in porous media are cylindrical in shape,

$$\Delta P = -\frac{2\gamma cos\theta}{R} \tag{4-3}$$

where *ΔP* is the pressure difference across the curved mercury interface (dyne/cm^2); *γ* is the surface tension of mercury (485 dynes/cm); *θ* is the contact angle (130°) between mercury and the porous media, as reported by Ellison et al. [24]; *R* is the corresponding pore radius (cm).

Micromeritics AutoPore IV 9510, the instrument used to perform MIP tests in this work, can generate pressure as high as 413 MPa (60,000 psia) during high-pressure analysis. According to Eq. (4-3), the pore diameter corresponding to this pressure is about 3 nm. The largest pore diameter measurable by MIP during low-pressure analysis is about 300 microns.

However, MIP testing has its shortcomings. Shi and Winslow [77] pointed out that changes of contact angle and damage to cement paste during the intrusion process should be considered, and that this may complicate MIP data processing. The ideal cylindrical pore shape may not be true [71], and an ink-bottle effect in MIP has been reported by many researchers [60]. The ink-bottle effect will result in an underestimation of large pores [92].

4.4.2.2. Determination of gas diffusivity from MIP data

Gas diffusion within pore spaces usually has two forms: Knudsen diffusion and normal diffusion [25]. The type of diffusion likely to be dominant depends on the relative length of the pore diameter and the mean free path of the gas molecule [59]. If the mean free path of the gas molecule is much larger than the pore diameter it passes through, then the collision of the gas molecules with the pore walls (i.e., Knudsen diffusion) will be the dominant process. In contrast, if the mean free path is much smaller than the pore diameter, the collisions between gas molecules (normal diffusion) will control the diffusion process, while the Knudsen diffusion is negligible. However, in many real situations these two diffusion mechanisms can simultaneously contribute to the gas diffusion in pore spaces.

For convenience, we arbitrarily chose O_2 with D_a = 2.04×10^{-5} m^2/s as the pseudo gas in the derivation process of this work. The mean free path of oxygen at standard ambient temperature and pressure (25 ºC, 1 bar) is about 0.073 µm and our MIP results show that the average pore sizes of most samples are at or below this length scale (Table 4-3). Because of this, Knudsen diffusion is considered in order to accurately predict diffusivity; this is shown in Eq. (4-4), which is known as the Bosanquet relation [67],

$$\frac{1}{D} = \frac{1}{D_a} + \frac{1}{D_{KA}} \tag{4-4}$$

where D is the gas diffusion coefficient [L^2 T^{-1}]; D_a denotes the gas diffusion coefficient in air [L^2 T^{-1}]; and D_{KA} is the Knudsen diffusion coefficient [L^2 T^{-1}].

The Knudsen diffusion coefficient, D_{KA}, depends on the temperature, molecular weight of gas (O_2) and average pore size of the porous medium, as expressed by Eq. (4-5) [17, 41, 74],

$$D_{KA} = 48.5 d_a \sqrt{\frac{T}{M}} \tag{4-5}$$

where T is absolute temperature (K); M is molecular weight of gas (g/mol); and d_a is the average pore diameter (m) that is calculated according to the following equation in MIP,

$$d_a = \frac{4V}{A} \times 10^{-6} \tag{4-6}$$

Where V is the total intrusion volume (mL/g); and A is the total pore area (m^2/g).

The effective diffusion coefficient was calculated according to the following equation [13, 25, 74],

$$D_e = \frac{\emptyset_a}{\tau} D \tag{4-7}$$

where τ is the tortuosity factor given by Carniglia [13] as follows,

$$\tau = 2.23 - 1.13\emptyset_a \quad \text{(applicable for } 0.05 \le \emptyset_a \le 0.95\text{)} \tag{4-8}$$

We should point out that the derivation of Eq. (4-8) is based on the assumption that cylindrical diffusion paths prevail in the given porous media [13].

In summary, after obtaining the average pore size and porosity from MIP tests, we were able to calculate gas diffusivity according to Eqs. (4-2), (4-4)–(4-8).

4.4.2.3. Permeability calculation from MIP data

Absolute (or intrinsic) permeability, a measure of the relative ease with which a porous medium can transmit a fluid under a potential gradient, is only a property of the porous medium and depends on the pore structure. Many researchers have attempted to derive permeability from MIP data [42-44, 82]. Among them, Katz and Thompson [42, 43] introduced the following equation (referred as KT method hereafter) to calculate the air permeability based on MIP data,

$$k = \frac{1}{89}(L_{max})^2\left(\frac{L_{max}}{L_c}\right)\phi S(L_{max}) \tag{4-9}$$

where k is air permeability (*D*arcy); L_{max} is the pore diameter (μm) at which hydraulic conductance is maximum; L_c is the characteristic length (μm) which is the pore diameter corresponding to the threshold pressure P_t; ϕ is porosity; and $S(L_{max})$ represents the fraction of connected pore space composed of pore width of size L_{max} and larger.

Webb [87] described the KT method (Eq. (4-9)) in detail for predicting permeability; we obtained the permeability of each sample according to the KT method. The relationship between permeability and porosity will be presented in the Results and Discussion section.

4.5 Results and Discussion

4.5.1. Repeatability of MIP Tests

Berea sandstone and concrete samples were selected for triplicate MIP testing and the remaining samples were tested only once. Ideally, a repeatability test should be carried out on the same sample as previously tested. This is not possible in the case of MIP testing, as the samples remain contaminated with mercury after any MIP test, and thus cannot be used in a subsequent MIP test. Therefore, we chose three representative samples from the same rock type or building material to evaluate the repeatability of MIP. The experimental result of triplicate MIP tests performed on Berea sandstone and concrete are shown in Figure 4-1, and the pore-size results of the repeatability tests are summarized in Table 4-2.

In Figure 4-1, the cumulative intrusion curves of Berea sandstone 2 and 3 (B2 and B3) are overlapped with each other while Berea sandstone 1 (B1) shows different behavior. This is in accordance with Table 4-2, in which the average pore diameter of B1 is smaller than B2 and B3. This difference probably reflects the heterogeneity of the Berea sandstone. The results of the three samples of concrete are acceptable considering the small pore sizes and heterogeneity of concrete.

4.5.2. Gas Diffusivity

Table 4-3 presents our results of several important parameters, such as diffusivity (*D'*) and the cementation factor (m values), for the total of 14 samples. Among consolidated samples, Berea sandstone has the highest diffusivity (*D'*= 0.104) while tuff has the lowest (*D'* = 0.007). Peng et al. [65] measured the effective diffusion coefficients of the same samples using the diffusion chamber method with oxygen. The comparison of results from the two approaches is shown in Figure 4-2. Except for one sample of unconsolidated sediment (size fraction 500 μm-2 mm) which shows a marked deviation, and limestone which was not available in Peng et al. [65], most of our results are distributed equally near the straight line with slope=1. This supports the validity of the derivation method of determining effective diffusion coefficient described in this work. Note that the unconsolidated sediment samples were compacted in the gas diffusion chamber method [65], while they were loosely placed into the penetrometer for the MIP tests. The difference in packing and porosity could contribute to the difference in obtained diffusivity for these sediment samples.

Table 4-2 Results of Repeatability Tests

Sample	MIP test	Porosity (%)		d_{50} (µm)		Average pore diameter d_a (µm)	
			avg±stan. dev.		avg±stan. dev.		avg±stan. dev.
Berea sandstone	1	24.845	22.865±1.724	22.982	23.776±0.876	0.071	1.339±1.098
	2	22.051		23.631		1.954	
	3	21.698		24.716		1.992	
Concrete	1	20.811	21.077±0.239	0.140	0.161±0.018	0.036	0.059±0.023
	2	21.273		0.171		0.081	
	3	21.148		0.171		0.059	

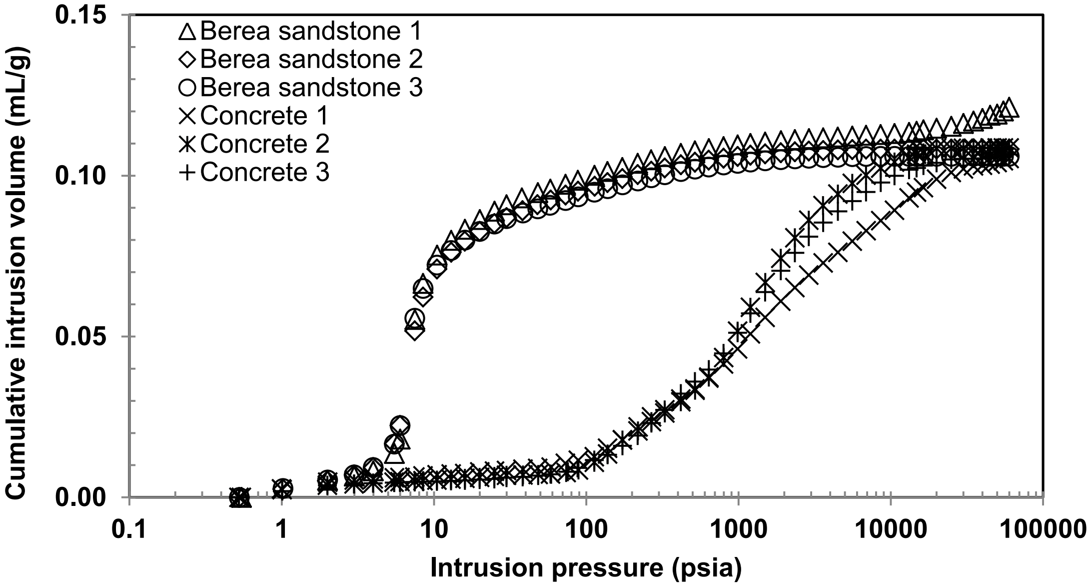

Figure 4-1 Cumulative Intrusion Volume vs. Intrusion Pressure for Berea Sandstone

Table 4-3 Porosity, Average Pore Diameter, Permeability, Effective Diffusion Coefficient, Diffusivity and m Values of 14 Samples

Sample	Porosity[a]	d_a[a] (μm)	Permeability (mdarcy)	D_e[b] (m^2/s)	D'[c]	m
Concrete 1	0.208	0.0357	1.45E-02	4.36E-07	0.021	2.45
Red brick	0.212	0.7345	1.42E+00	1.83E-06	0.090	1.56
Limestone	0.145	0.3656	3.78E+01	1.04E-06	0.051	1.54
Dolomite	0.091	0.1361	4.09E-01	4.35E-07	0.021	1.61
Indiana Sandstone	0.167	0.2088	1.92E+02	1.01E-06	0.049	1.68
Berea Sandstone 2	0.221	1.9539	5.71E+02	2.12E-06	0.104	1.50
Gray Chalk	0.320	0.1149	1.22E-01	1.59E-06	0.078	2.24
White Chalk	0.438	0.0915	2.23E-01	2.05E-06	0.100	2.78
Tuff	0.096	0.0252	7.33E-04	1.43E-07	0.007	2.12
Mudstone	0.196	0.0282	2.26E-03	3.37E-07	0.017	2.52
Hanford < 2mm	0.401	0.0937	3.69E+02	1.86E-06	0.091	2.62
Hanford 500 um-2 mm	0.137	0.0380	3.23E-01	2.89E-07	0.014	2.14
Hanford 75-500 um	0.480	0.1590	7.06E+02	3.10E-06	0.152	2.57
Hanford < 75um	0.586	0.1947	2.83E+01	4.46E-06	0.219	2.85

[a] Obtained from MIP.
[b] Calculated at temperature 20 ºC for oxygen.
[c] Calculated according to Eq. (4-2) with $D_a = 2.04\times10^{-5}$ m^2/s for oxygen.

4.5.3. Correlation of Gas Diffusivity with Porosity and Permeability

The exponential relationship between permeability and diffusivity, as shown in Figure 4-3, is weak with a correlation coefficient value of R^2=0.549. However, it indeed indicates an increasing trend of diffusivity with the increase of permeability.

According to Eq. (4-2), we should obtain a linear relationship if we plot diffusivity versus porosity in log scale and the slope of the plot should give the value of m. Figure 4-4 shows the relationship between *D'* and porosity for our samples. The samples can be divided into two groups according to the different slope (m) value. One group, with m =

1.5, includes dolomite, limestone, Indiana sandstone, Berea sandstone and red brick and the remaining samples fall into another group with m = 2.5.

All four samples of unconsolidated sediment show relatively high m values (from 2.1 to 2.8), and the finer sediment tends to exhibit a larger m value, which is consistent with the conclusion of Peng et al. [65]. For consolidated samples, we plotted the diffusivity versus median pore diameter (d_{50}) and the two sample groups are shown with different legends in Figure 4-5. We found that these two groups could also be separated by a cut-off d_{50} value of ~0.5 μm. All the samples in the group with m=1.5 have a relatively large d_{50} (>0.5μm), while the samples of the m=2.5 group have a smaller d_{50} (<0.5μm); in other words, the tighter samples with d_{50}<0.5 μm tend to have the larger m value of 2.5. Compared with the scattered samples of the group with m=1.5 (R^2=0.254), the tight samples exhibit a more organized behavior and display an exponential relationship between D' and d_{50} as shown in Figure 4-5. This relationship can be summarized as

$$D' = 0.25{d_{50}}^{1.017} \quad (4\text{-}10)$$

where D' denotes diffusivity (dimensionless) and d_{50} is the median pore diameter in μm.

Although the MIP-derived gas diffusivities of building materials and unconsolidated sediments are comparable with the measured data (Figure 4-2), the complexity of factitious building materials and the instability of unconsolidated sediments make it difficult to draw further conclusions, and interpretation of the complicated pore structures of these two types of porous medium is beyond the scope of this work. Accordingly the emphasis in the remainder of this section will be on the eight consolidated rock samples.

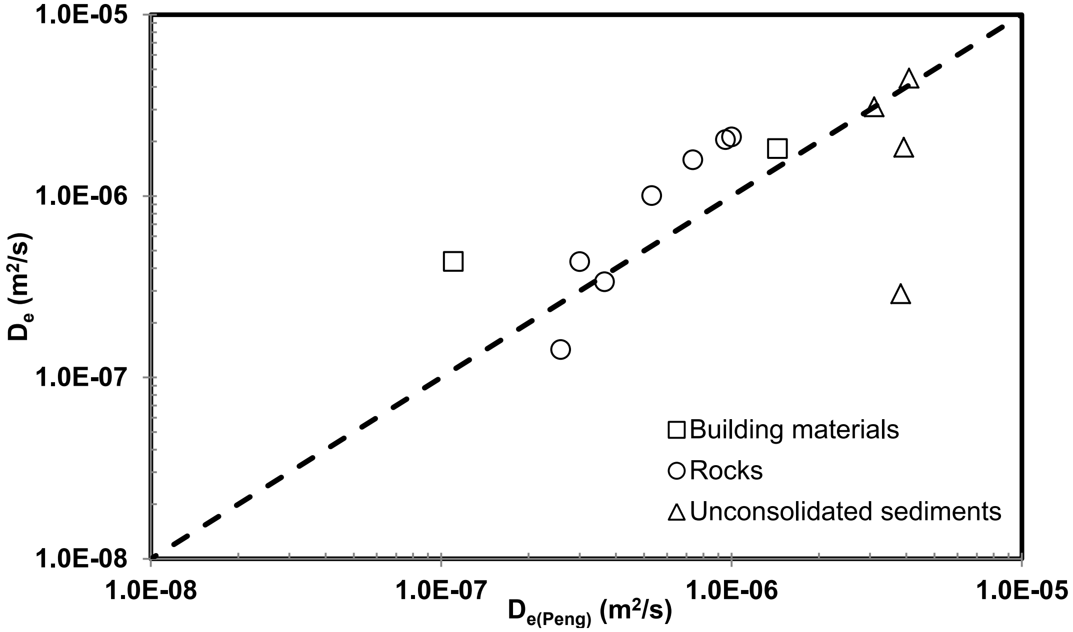

Figure 4-2 Comparison between Effective Diffusion Coefficients Obtained in This Work

(D_e) and from Reference ($D_{e(Peng)}$)

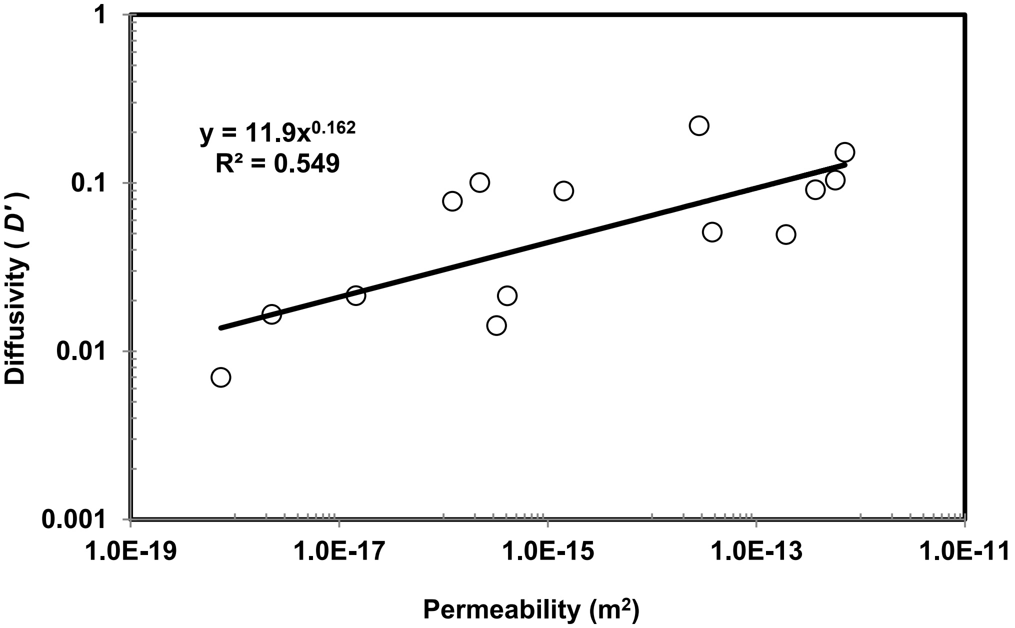

Figure 4-3 Diffusivity (*D'*) vs. Permeability

The relationship between permeability and porosity has been investigated and presented by many researchers [15, 54, 84]. We plot the permeability versus porosity for eight rock samples together with two building materials in Figure 4-6. The results show two different exponential relationships with relatively high R^2 (>0.9) for the two groups of samples with different m values. Again, dolomite, limestone, Indiana sandstone and Berea sandstone fall in the same group (m=1.5), while tuff, mudstone, gray chalk and white chalk belong to the other group (m=2.5).

For the sample group with m=1.5, the following relationship exists,

$$k = 4 \times 10^{-7} \emptyset_a^{\ 8.53} \tag{4-11}$$

where k is permeability in m^2 and Φ_a is air-filled porosity.

For the group with m=2.5, the relationship is

$$k = 6 \times 10^{-15} \emptyset_a^{\ 4.10} \tag{4-12}$$.

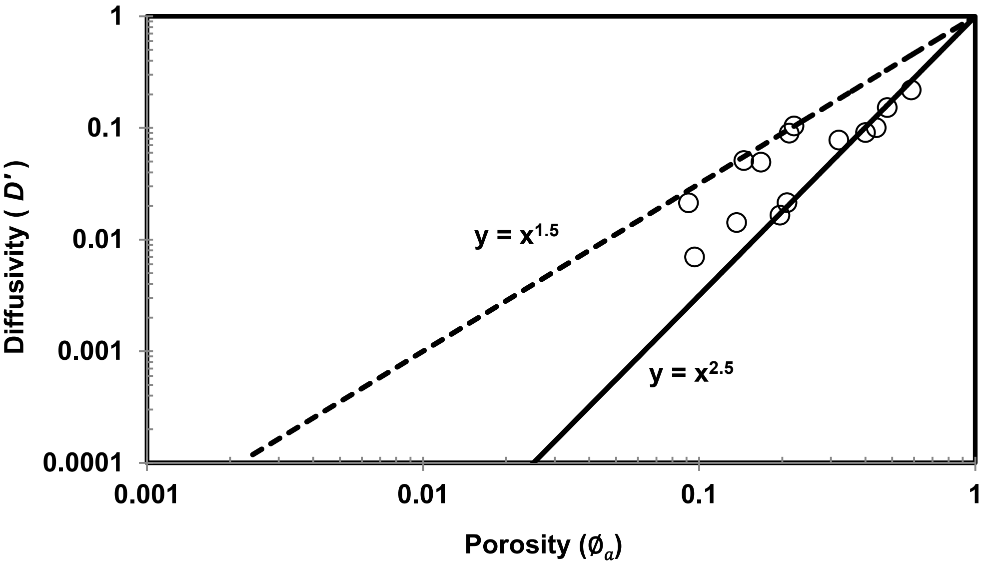

Figure 4-4 Diffusivity (D') vs. Porosity ($\emptyset_a$) for Our Samples (two groups are divided according to the m value)

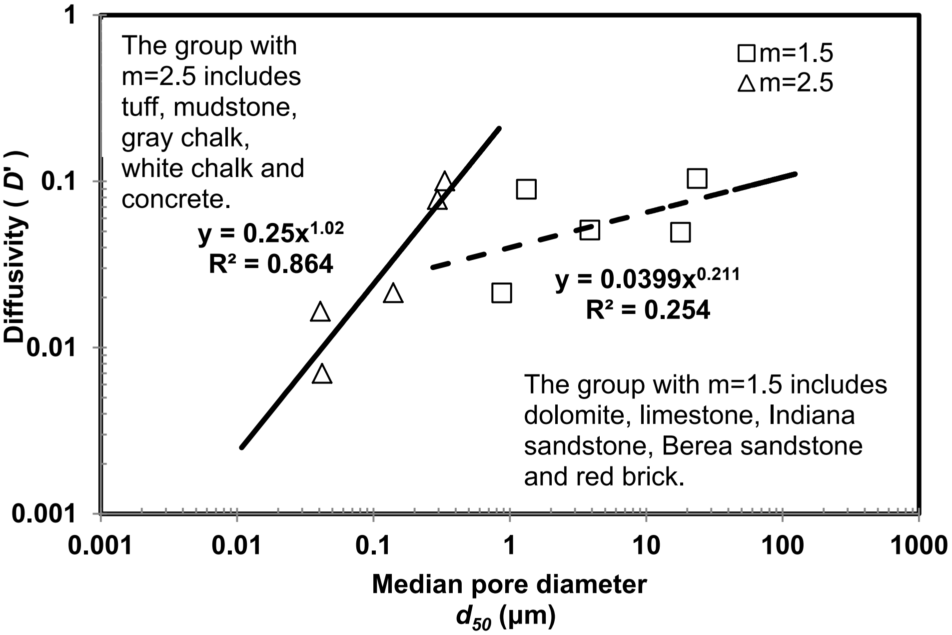

Figure 4-5 Diffusivity (*D'*) vs. Median Pore Diameter (d_{50}) for Consolidated Materials

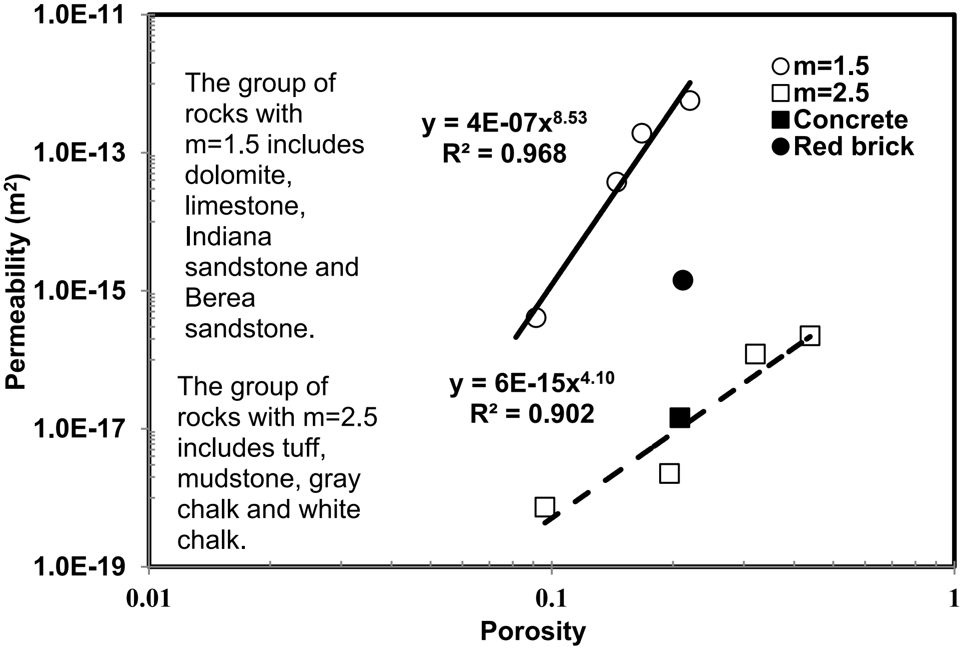

Figure 4-6 Permeability vs. Porosity for Consolidated Materials

4.6 Conclusion

The objective of this work was to derive gas diffusivity from MIP data and to explore the correlation of diffusivity with permeability and porosity. The repeatability of MIP determinations was evaluated using Berea sandstone and concrete. In terms of average pore size, our results show that the consideration of Knudsen effect in many rocks is necessary. The effective diffusion coefficients (D_e) of three types of porous media (two building materials, eight consolidated rocks and four unconsolidated sediments) were calculated with established equations, using the information on average pore diameter (d_a) and porosity ($\emptyset_a$), both of which are easily obtained by MIP. The results are basically in line with the experimental values obtained from gas diffusion tests. It should be pointed out that the method used to calculate D_e in this work is only applicable to samples with porosity between 0.05 and 0.95, as indicated in Eq. (4-8) of Carniglia [13]. However, except for extremely tight rocks such as granite, this method still has a wide applicability. Usually, one MIP test can be completed within two hours, which enhances the applicability of this method.

An increasing trend of diffusivity with increasing permeability was observable in our results, although the correlation was weak, as shown in Figure 4-3. Diffusivity, calculated according to Eq. (4-2), was also used to obtain the m value, which is closely related to the pore structure. Two groups of samples were divided according to the m values (m=1.5 vs. m=2.5). For the consolidated samples, these two groups could be further differentiated from each other according to the median pore diameter (d_{50}) obtained from MIP. When d_{50} is larger than ~0.5 μm, the samples belong to the group with m=1.5. Conversely, if d_{50} is less than ~0.5 μm the sample probably has an m value of 2.5 and the diffusivity of this sample can be estimated according to Eq. (4-10). Moreover, the relationship between permeability and porosity was investigated for eight rock samples. Again, dolomite, limestone, Indiana sandstone and Berea sandstone in the group with m=1.5 exhibited similar behavior, which can be expressed by Eq. (4-11), while tuff, mudstone, gray chalk and white chalk, all of which belonged to the group with m=2.5, shared the same power-law-form of Eq. (4-12).

Chapter 5

Wettability and Pore Connectivity of Barnett Shale at Different Depths: Investigation from Directional Spontaneous Imbibition and Mercury Intrusion Porosimetry

5.1 Abstract

The Barnett shale, as one of the nation’s most prolific unconventional reservoirs, has attracted the attention of scientists and engineers, and has been characterized from many different perspectives. For several decades, imbibition experiments have been conducted by many investigators to study the factors influencing hydrocarbon recovery, and mercury intrusion porosimetry (MIP) has been applied in pore structure characterization. The present study examines the spontaneous imbibition behavior of Barnett shale samples taken from four different depths, using two types of imbibing fluid (water and n-decane), and characterizes the pore structure of Barnett shale using MIP as a supplemental method of investigation. The shale samples were taken from a well in Wise County, Texas, within the Fort Worth Basin, at depths below land surface of 7136 ft (2175 m), 7169 ft (2185 m), 7199 ft (2194 m) and 7219 ft (2200 m). During the imbibition experiments, all sides of the sample prisms were coated with quick-cure epoxy except top and bottom, so as to generate co-current imbibition in the vertical direction. The scaling method proposed by Ma et al. [55] was used to permit comparison of water and n-decane imbibition into Barnett samples from the same depth, and to gain insight into the effect of wettability on imbibition behavior. In addition, imbibition experiments were conducted in two directions, parallel to and transverse to the bedding planes of the samples, by orienting and epoxy-coating the samples differently. The observed directional dependency of fluid imbibition contributed to the interpretation of wettability conditions. Information on pore-throat size distribution was obtained from MIP and a

comparison was made among the samples from different depths. Our results show that wettability significantly affects imbibition behavior and that the samples tested in this study can be divided into three categories based on wettability condition (strongly water-wet, intermediate-wet and oil-wet). In addition, the low pore connectivity of Barnett shale is confirmed by both water imbibition and MIP results.

5.2 Introduction

With the development of new drilling and fracturing technologies, the production of shale gas has significantly increased and it is predicted that shale gas will become the source of 49% of total dry gas production in the USA by 2035 [5]. Understanding the pore structure of these extremely low-permeability (usually in the nano-darcy range) reservoirs has been a challenging task due to the limitation of applicable characterization tools and techniques. Recently the Barnett shale, the first developed shale play and one of the most successful unconventional reservoirs in the world, has been the subject of many studies incorporating different approaches to the investigation of pore structure characteristics. For example, Slatt and O'Brien [79] characterized the pore types of the Barnett and Woodford gas shales using scanning electron microscopy. Chalmers et al. [14] investigated the pore systems of Barnett shale using multiple approaches, including mercury intrusion porosimetry (MIP). In addition, Hu et al. [40] investigated the low pore connectivity of Barnett shale using spontaneous water imbibiton, tracer concentration profiles, and imaging in combination with network modeling. The present study includes imbibition experiments on Barnett shale samples from different depths in a single well, characterizing the imbibition behavior with respect to bedding plane orientation and wettability. The experiments included imbibition in two different directions (parallel to and transverse to the bedding plane); in each individual experiment, either water or n-decane was used as the imbibing fluid. We also performed MIP tests on the samples to measure porosity and to investigate pore connectivity by deriving tortuosity values from the MIP data.

5.2.1. Barnett Shale

Located in at least 17-county area of the Fort Worth Basin in north-central Texas, the Barnett Shale is a Mississippian-age marine shelf deposit, and ranges in thickness from 200 ft in the southwest region to 1,000 ft to the northeast. The Barnett Formation could be divided into three members where the Forestburg limestone is present: upper Barnett section, Forestburg limestone and the lower Barnett section. Upper and lower Barnett sections mainly consist of a variety of siliceous mudstones with less abundant interbedded lime mudstones and skeletal packstones, while the Forestburg section is composed of laminated, argillaceous lime mudstone [49].

X-ray powder diffraction analyses of 35 cuttings from three wells in Wise and Denton counties give the following shale composition by weight: 45-55% silts (mostly quartz and some plagioclase); 15-25% carbonates (mostly calcite, some dolomite, and siderite); 20-35% clay minerals; and 2-6% pyrite [49, 91]. Total organic carbon ranges from 3.5 to 4.5% by weight, which translates to 7-9% by volume because the organic matter has a lower density than the minerals. The organic matter in the shale is mainly type II kerogen, which can generate both oil and gas directly [91].

In Wise County, Texas, the Barnett Shale has a net thickness of 50-200 ft, TOC 4.5%, gas-filled porosity of 2.5% and water-filled porosity of 1.9%, adsorbed gas content at 20% [18]. The Texas United 1 Blakely core (120 ft; 37 m), located in Wise County, within the Fort Worth Basin, includes part of the upper Barnett section (from 7105 to 7117 ft), the Forestburg limestone (from 7117 to 7155 ft), and the upper part of the lower Barnett section (from 7155 to 7225 ft) [49]. Loucks and Ruppel [49] also found a well-developed hardground at 7198 ft (2193 m) in the Blakely core and pointed out that this hardground has well-developed phosphate-coated grains (ooids) and massive pyrite replacement.

The shale samples used here were taken from this Blakely well, at depths below land surface of 7136 ft (2175 m), 7169 ft (2185 m), 7199 ft (2194 m) and 7219 ft (2200 m) and the photos of these core samples are listed in Figure 5-1.

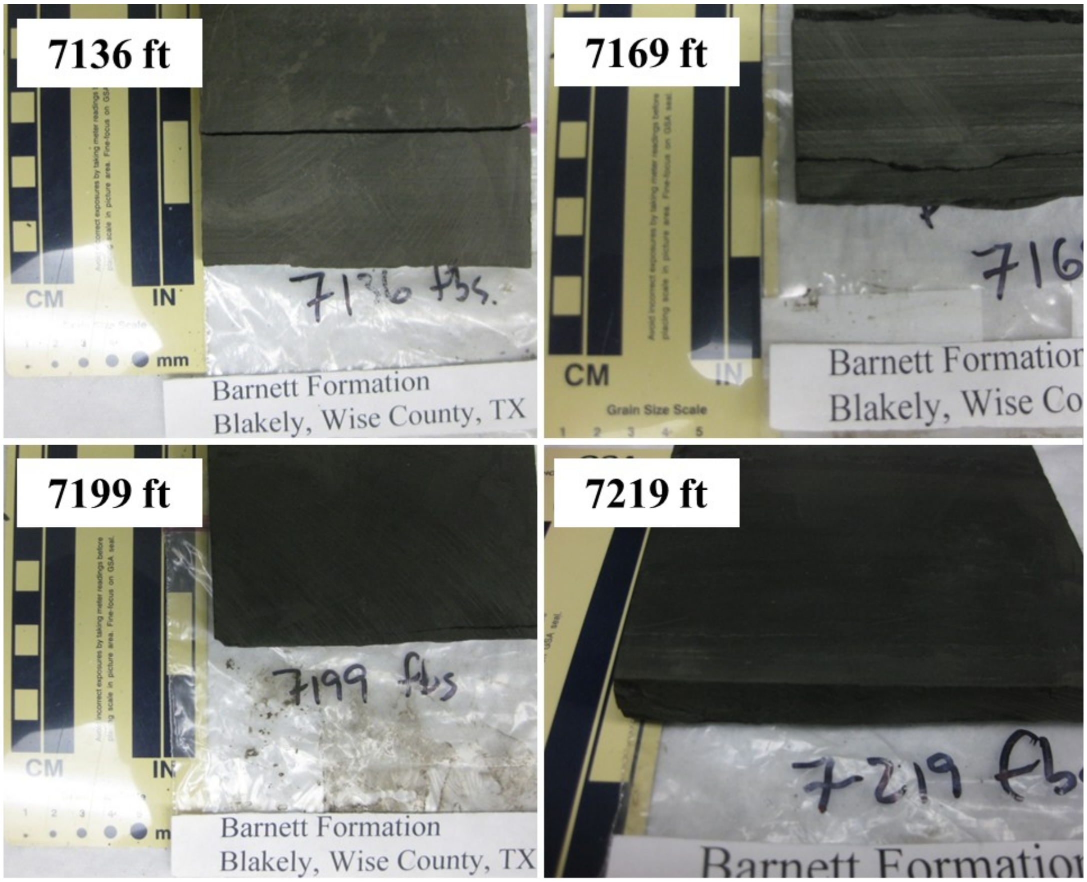

Figure 5-1 Photos of Barnett Shale Core Samples from Different Depths

5.2.2. Wettability

Wettability shows the tendency of solid surfaces to be preferentially wet by one fluid phase. The wettability of reservoir rock is a critical factor influencing the petroleum recovery process; the Amott test [4] and the U.S. Bureau of Mines (USBM) test [21] are the most commonly used methods of determining the wettability of oil/brine/rock systems. However, the extremely low permeability of shales, coupled with the dependence of these two methods on capillary pressure and microscopic displacement efficiency, makes the measurement of wettability of shales using these two methods difficult. Wettability could also be evaluated by directly measuring contact angle, but the problems of reproducibility (possibly caused by surface contamination, surface roughness, heterogeneity in chemical composition and so on) render this method challenging [61]. Recently surface forces and NMR have been discussed in the literature as supplemental approaches in characterizing the wettability of shale [81, 83]. Although the idea of determining wettability from spontaneous imbibition has been discussed by many researchers [19, 61, 63], most of the research has focused on sandstone with relatively high porosity and permeability, and relatively little attention has been paid to tight shales. Makhanov et al. [56] conducted an experimental study of spontaneous imbibition into Horn River shale samples from different depths. They found that the studied shale samples were oil-wet, based on contact angle measurement; they further noted that fluid imbibition into Horn River shale showed strong directional dependency. This directional dependency is also observed in Barnett shale and it is used to interpret wettability condition here. The work reported herein represents the first published attempt to characterize qualitatively the wettability of Barnett shale from different depths by conducting imbibition experiments along different directions, using two types of imbibing fluids, and using the scaling method proposed by Ma et al. [55] to interpret imbibition data.

5.2.3. Spontaneous Imbibition

Spontaneous imbibition (SI) is a capillary-force controlled process during which a wetting fluid displaces a non-wetting fluid under the influence of capillary suction only. In the process of oil/gas recovery from fractured reservoirs, water is imbibed into the rock matrix blocks from the fracture system by SI, with the result that oil /gas in the matrix is displaced by the water. As a result, the oil/gas production rate is strongly dependent on the SI process, and extensive research has been undertaken to investigate that process [32, 47, 76, 80].

Handy [34] proposed the following equation (Eq. (5-1)) to describe the SI process in a water-air system in which imbibition occurs vertically upward and the gravitational force can be neglected:

$$Q_w^2 = (\frac{2P_c k_w \emptyset A^2 S_w}{\mu_w})t \tag{5-1}$$

where Q_w is the volume of water imbibed into the core sample in cm^3; P_c is the capillary pressure (atm); k_w is the effective permeability in darcies; $\emptyset$ is fractional porosity; A is the cross-sectional area of the core in cm^2; S_w is fractional water content of the pore spaces; t is imbibition time in seconds; and μ_w is the viscosity of water in centipoises.

Handy's equation can be simply expressed as,

$$H = at^{0.5} \tag{5-2}$$

Where H is cumulative imbibition height which equals Q_w/A; a is a constant.

Handy's equation (Eq. (5-1)) is based on three assumptions (1) the water imbibes in a piston-like manner; (2) the pressure gradient in the gas phase ahead the water front can be neglected; and (3) gravity forces are much less than capillary forces.

Handy's equation implies that the cumulative imbibition height is proportional to the square root of the imbibition time, so that theoretically a slope of 0.5 should be obtained if cumulative imbibition height is plotted vs. imbibition time on log-log coordinates. For imbibition into Indiana sandstone, metagraywacke, and Barnett shale, Hu et al. [40] reported three types of imbibition slope, the theoretical value of 0.5, but also 0.26, and 0.26 transitioning to 0.5). Percolation theory suggests that the lower slope values may be an indication of low pore connectivity.

Wettability, boundary conditions, shape factor, viscosities of fluids, interfacial tension, initial wetting fluid saturation, pore structure of the rock, and temperature are generally considered the important factors influencing the imbibition process [57, 62, 89]. Scaling of SI behavior is generally recognized as an effective method of investigating the factors controlling the SI process. Mattax and Kyte [58] proposed the following scaling equation,

$$t_D = t\sqrt{\frac{k}{\emptyset}}\frac{\sigma}{\mu_w L^2} \quad (5\text{-}3)$$

where t_D is dimensionless time; t is imbibition time (s); k is absolute permeability (m^2); $\emptyset$ is fractional pososity; σ is interfacial tension (N/m) between wetting and non-wetting phases; μ_w is viscosity of imbibing water (Pa·s); and L is sample length (m).

Zhang et al. [90] revised this equation, using the geometric mean of the fluid viscosities to account for variations in the viscosity of the displaced phase; they emphasize that the use of this new term is empirical, with no theoretical basis. Another new term, called characteristic length (L_c), was proposed by Ma et al. [55] to account for different sample shapes and boundary conditions. After these two major revisions, Eq. (5-3) becomes

$$t_D = t\sqrt{\frac{k}{\emptyset}}\frac{\sigma}{\sqrt{\mu_{we}\mu_{nw}}L_c^2} \quad (5\text{-}4)$$

where μ_{we} is the viscosity of the wetting phase (Pa·s); μ_{nw} is the viscosity of the non-wetting phase (Pa·s); L_c is the characteristic length (m) which is defined by the following equation,

$$L_c = \sqrt{\frac{V_b}{\sum_{i=1}^{n} A_i / l_{A_i}}} \tag{5-5}$$

where V_b is the bulk volume of the matrix (m^3); n is the total number of surfaces open to imbibition; Ai is the area open to imbibition in the ith direction (m^2); l_{A_i} is the distance that the imbibition front travels from the imbibition face to the non-flow boundary (m).

Although Eq. (5-4) has a more generalized form than Eq. (5-3), there are still several limitations for the dimensionless time as calculated by Eq. (5-4). As mentioned by Li [47], these limitations include that (1) wettability must be the same; (2) relative permeability functions must be identical; (3) capillary pressure functions must be identically proportional to interfacial tension; (4) initial fluid distributions must be duplicated; and (5) gravity must be neglected.

By using Eq. (5-4), imbibition data can be adjusted to compensate for differences in pore structure, viscosity, interfacial tension and boundary conditions; wettability, the remaining factor, is not taken into account when the imbibition of different fluids into the same sample is considered. As a result, for the same sample the difference of imbibition behavior is mainly determined by wettability after scaling with Eq. (5-4).

5.2.4. Theory of Mercury Intrusion Porosimetry (MIP)

Mercury, as a non-wetting fluid to most geological materials, will not invade pores unless it is applied with external pressure. Washburn [86] developed the following equation which is often applied as the basic theory for MIP, under the assumption that all pores in the medium are cylindrical,

$$\Delta P = -\frac{2\gamma cos\theta}{R} \tag{5-6}$$

where *ΔP* is the pressure difference across the curved mercury interface (dyne/cm^2); *γ* is the surface tension of mercury (485 dynes/cm); *θ* is the contact angle (130º) between mercury and the porous medium; and *R* is the corresponding pore radius (cm).

With the increase of applied pressure during the intrusion process, the volume change of intruded mercury will be recorded by MIP as an intrusion curve and the pore-throat size distribution can be derived from this intrusion curve according to Washburn's equation (Eq. (5-6)). Many studies have been conducted to derive permeability from MIP data [42-44, 82]. Among them, Katz and Thompson [42, 43] introduced the following equation to estimate permeability based on the MIP data,

$$k = \frac{1}{89}(L_{max})^2(L_{max}/L_c)\emptyset S(L_{max}) \tag{5-7}$$

where *k* is air permeability (Darcies); L_{max} (μm) is the pore-throat diameter at which hydraulic conductance is maximum; L_c (μm) is the characteristic length which is the pore-throat diameter corresponding to the threshold pressure P_t (psia) and P_t is determined at the inflection point of the cumulative intrusion curve; ∅ is porosity; $S(L_{max})$ represents the fraction of connected pore space composed of pore width of size L_{max} and larger.

The process of using the Katz and Thompson (KT) method (Eq. (5-7)) to calculate permeability is described in detail by Gao and Hu [28]; in the present study we calculate the permeability of our samples using the KT method.

Tortuosity, another important parameter which may indicate pore connectivity, can also be derived from MIP data [33, 87]

$$\tau = \sqrt{\frac{\rho}{24k(1+\rho V_{tot})}\int_{\eta=r_c,min}^{\eta=r_c,max}\eta^2 f_V(\eta)d\eta} \tag{5-8}$$

where ρ is fluid density (mass/volume); *k* is permeability (area); V_{tot} is total pore volume (volume/mass); $\int_{\eta=r_c,min}^{\eta=r_c,max} \eta^2 f_V(\eta) d\eta$ is pore-throat volume distribution by pore-throat size; τ is tortuosity which is defined by the following equation,

$$\tau = \frac{l_e}{l} \tag{5-9}$$

where l_e is actual distance traveled by a fluid particle as it moves between two points in a porous medium which are separated by a straight line distance l .

Despite the importance of diffusion to gas production, there is no systematic study examining permeability and diffusivity of the Barnett shale [11]; this work provides the first measurements of chemical diffusivity (in terms of tortuosity) of shale samples.

5.3 Imbibition and MIP Experiments

We performed SI and MIP tests on Barnett shale core samples from the Blakely well [50] (API 497-33041, Wise County, TX), taken from the following depths: 7136 ft (2175 m), 7169 ft (2185 m), 7199 ft (2194 m) and 7219 ft (2200 m).

For the imbibition experiments, all the samples were cut into rectangular prisms and all sides (except top and bottom) were coated with quick-cure transparent epoxy to avoid condensation/evaporation of the imbibing fluid (water or n-decane) from the side surfaces of the samples. The imbibition apparatus was already shown in Figure 2-1 (Gao and Hu [27]); the experimental procedure and the data processing method were described in detail by Hu et al. [39]. It should be noted that all the samples were oven-dried at 60 ºC for at least 48 hours before they subjected to the imbibition experiments in order to achieve a constant initial water saturation state. We used water and n-decane (oil phase) as the imbibing fluids during the imbibition experiments; the physical properties of these fluids are listed in Table 5-1. N-decane was used to probe the oil-wetting characteristics of the samples. Air was always treated as the displaced non-wetting phase in our imbibition experiments. During the water imbibition experiments, beakers of water were placed inside the experiment chamber to keep the humidity inside the chamber constant and these beakers were removed for the n-decane imbibition experiments because they could affect the n-decane imbibition process. As the wettability of the tested samples could be changed by n-decane imbibition, we did not perform triplicate tests on the same sample in the n-decane experiments, as we did for the water imbibition tests. Because of the layered characteristics of Barnett shale, we carried out imbibition experiments in different directions with respect to the bedding planes, by coating the sample surfaces differently, as shown in Figure 5-2; the symbols P and T are used herein to designate imbibition parallel to and transverse to the bedding, respectively. The dimensions of all the samples used in the imbibition experiments are listed in Table 5-2.

We used Micromeritics AutoPore IV 9510 to perform MIP tests in this work. The instrument is capable of generating pressures as high as 60,000 psia (413 MPa) during high-pressure analysis; the pore-throat diameter corresponding to this pressure according to Eq. (5-6) is about 3 nm. In contrast, the largest pore-throat diameter measurable by MIP during low-pressure analysis after pulling vacuum is about 300 microns. All the samples (mostly cube-sized, with the largest linear dimension of about 1.5 cm) were oven-dried at 60 ºC for at least 48 hours to remove moisture from the pore spaces, and were then cooled to room temperature (~23 ºC) in a desiccator before they were subjected to the MIP test. After obtaining the permeability using KT method, MIP instrument could produce the tortuosity values according to Eq. (5-8).

Table 5-1 The Physical Properties of Related Fluids

Fluid	Density (g /cm^3)	Viscosity (mPa·s)	Interfacial tension with air (mN/m)
Air	-	0.018	-
Water	1.00	1.002	72.0
n-decane	0.73	0.84	23.9

Table 5-2 Dimensions of Samples Used in SI Experiments

Sample depth (ft)	Porosity[a]	Sample ID[b]	Fluid used[c]	Length (cm)	Width (cm)	Height (cm)
7,136	0.0105	B7136PA	water and n-decane	1.7	1.7	1.2
		B7136TA	Water	1.4	1.7	1.7
		B7136TB	n-decane	1.5	1.7	1.4
7,169	0.0288	B7169PA	water and n-decane	1.2	1.8	1.3
		B7169TA	water and n-decane	1.4	1.8	1.8
		B7169PB	n-decane vapor	1.7	1.5	1.3
		B7169TB	n-decane vapor	1.8	1.4	1.3
7,199	0.0596	B7199PA	water and n-decane	1.7	1.7	1.2
		B7199TA	Water	1.2	1.7	1.7
		B7199TB	n-decane	1.7	1.3	3.9
7,219	0.0261	B7219PA	water and n-decane	1.7	1.7	1.4
		B7219TA	water and n-decane	1.4	1.7	1.9

[a] Porosity is measured by MIP.

[b] A and B stand for different samples.

[c] Where both water and n-decane SI experiments were performed on the same sample, the n-decane SI experiment was carried out after the water SI experiments were completed. Water imbibition was repeated at least three times on the same sample.

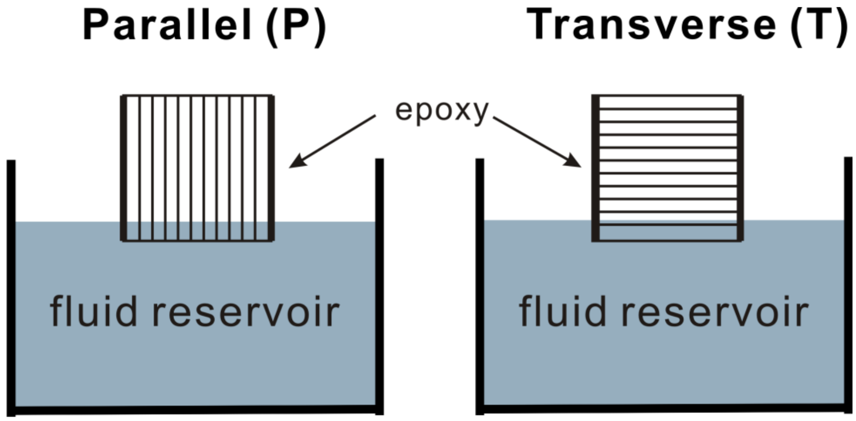

Figure 5-2 Parallel Sample (P) and Transverse Sample (T) in SI Experiments (Parallel lines within samples stand for bedding layers in Barnett shale)

5.4 Results and Discussion

5.4.1. Wettability Inferred from SI Experiments

As mentioned above, the wettability of the samples could be indicated from imbibition experiments after scaling the imbibition data using Eq. (5-4). In order to make a better comparison, a dimensionless weight was introduced as follows,

$$W_D = W/[\rho \emptyset V] \tag{5-10}$$

where W_D is the dimensionless weight; W is the imbibed weight of water or n-decane; ρ is the density of water or n-decane; $\emptyset$ is fractional porosity; and V is sample volume.

Both cumulative imbibition height and imbibition time were plotted in log-log scales for all the samples. The wettability of Barnett shale samples are qualitatively divided into three categories (oil-wet, strongly water-wet and intermediate-wet) based on the different imbibition behaviors observed. The imbibition slope together with imbibed weight is used to identify wettability conditions of our samples and the directional dependency of imbibition related to wettability is also discussed in the following subsections.

5.4.1.1. Oil-wet Barnett shale from the depth of 7136 ft (B7136)

Oil-wet samples are characterized by the higher n-decane imbibition slope compared with water imbibition for both P and T samples. During the initial thirty seconds or so of each SI experiment, the samples were not mechanically stable, but rather tended to vibrate slightly in the vertical direction. For times after this initial period of instability, a linear relationship was observed in the logarithmic plots of cumulative imbibition height versus imbibition time. For B7136 samples, the P and T samples show similar n-decane imbibition behavior (Figure 5-3). Both the B7136PA and B7136TB samples began to imbibe n-decane almost as soon as they contacted n-decane. The direction of flow relative to the bedding orientation had little effect on the n-decane imbibition curves, indicating that n-decane could readily imbibe either along or across the bedding planes.

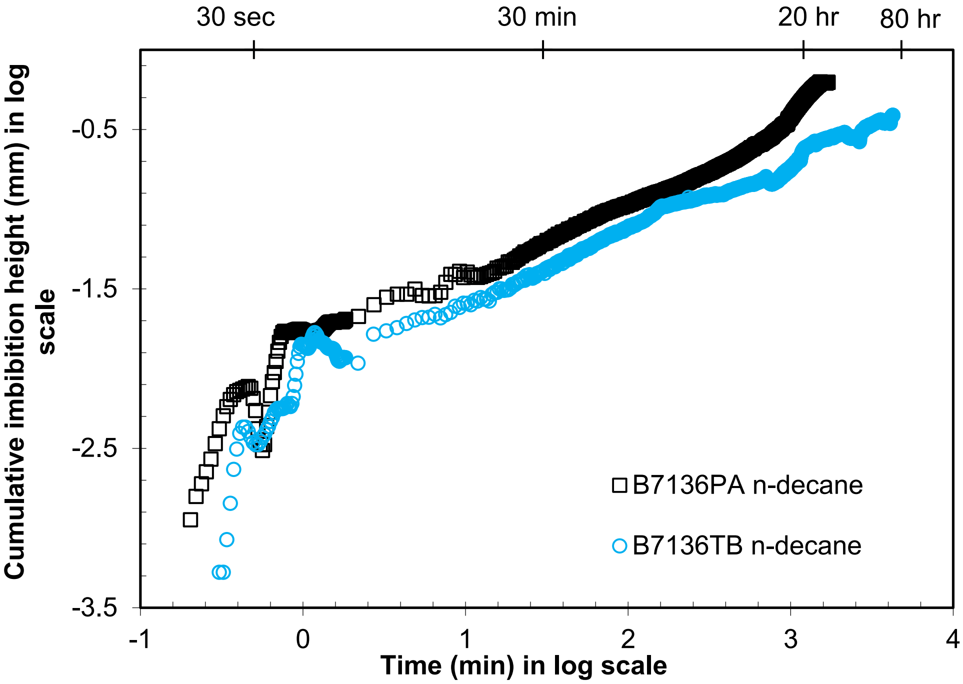

Figure 5-3 Cumulative *n*-decane Imbibition (mm) vs. Time (min) in Log Scales for B7136 Samples

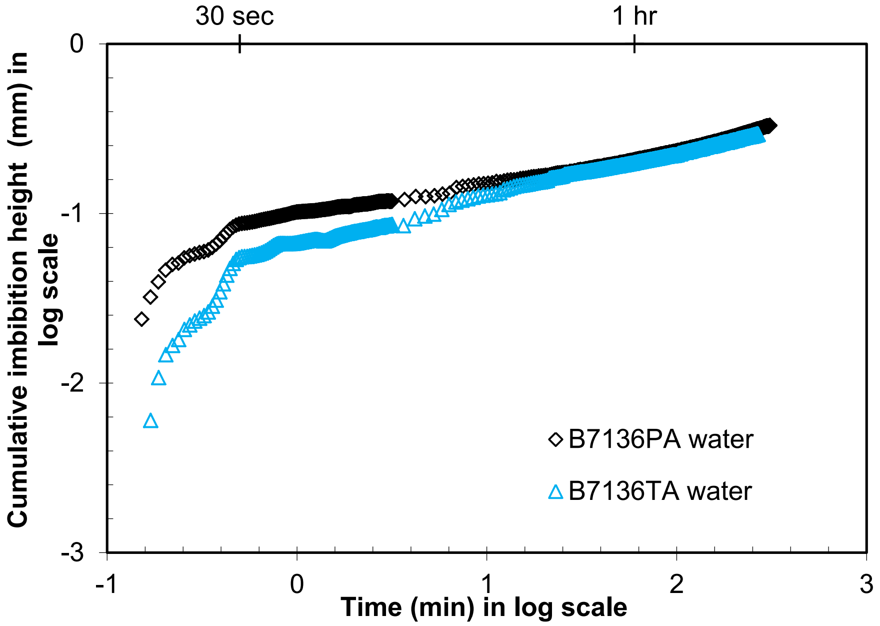

Figure 5-4 Cumulative Water Imbibition (mm) vs. Time (min) in Log Scales for B7136 Samples

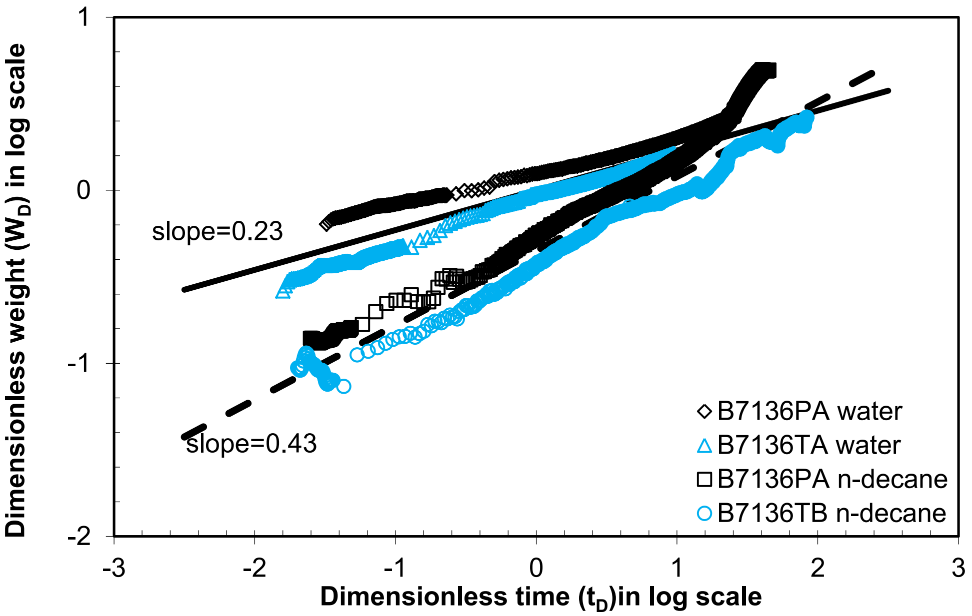

Figure 5-5 W_D vs t_D for B7136 Samples

It is not appropriate to compare directly water imbibition and n-decane imbibition curves, due to the different properties of the two fluids. For this reason the results of water imbibition experiments for B7136 samples are shown separately in Figure 5-4. The comparison between water and n-decane imbibition is made by plotting the dimensionless weight, $W_{D,}$ versus dimensionless time, $t_{D,}$ in log scale, as shown in Figure 5-5. The slope of n-decane imbibition for B7136PA and B7136TB is about 0.43 which is much higher than 0.23, the slope of water imbibition for B7136PA and B7136TA, which indicates the oil-wet property of B7136 samples.

5.4.1.2. Strongly water-wet Barnett shale from the depth of 7169 ft and 7219 ft (B7169 and B7219)

The most significant characteristic of the strongly water-wet category is the different n-decane imbibition behavior of the P and T samples. During the first 10 minutes, almost no n-decane was imbibed into B7169TA, while a relatively large amount of n-decane was taken up into B7169PA during the same period, as shown in Figure 5-6. We also performed n-decane vapor absorption experiments on B7169 P and T samples, during which the sample was suspended above the n-decane surface without submerging it into the n-decane reservoir; the results are also presented in Figure 5-6. The n-decane vapor absorption curves of the B7169 samples exhibited a shape similar to that of the n-decane imbibition curve for B7169TA, suggesting a possible explanation of the n-decane imbibition process in T samples. Because of the strongly water-wet nature of the medium, n-decane was not readily imbibed by the T samples of this category in the initial phase of the experiment; however, during this period, n-decane vapor may have been able to enter the pore space in sufficient quantity to alter the wettability toward a more oil-wet condition. If this in fact occurred, it would account for the increased imbibition of n-decane into the medium as the experiment continued.

In the case of the P samples of this category, however, the experimental results suggest different controlling conditions. The n-decane imbibition curve of B7169PA in fact appears much closer to an oil-wet imbibition curve. This is probably caused by n-decane migration along some visible cracks (about 0.1mm width as observed with microscopy) between adjacent parallel bedding planes. These cracks are probably the result of two mechanisms: (1) during the process of sedimentation and compaction, some cracks were naturally produced; (2) during the drilling process some cracks might be produced artificially as a result of pressure release.

In contrast to the n-decane imbibition experiments, no significant difference was observed between P and T results during water imbibition (Figure 5-7); this indicates that water may be imbibed with equal facility along or across the bedding planes, perhaps because of the strongly water-wet character of the samples. The water and n-decane imbibition curves after scaling are shown in Figures 5-8 and 5-9; the strongly water-wet condition appears to dominate the imbibition behavior of these samples.

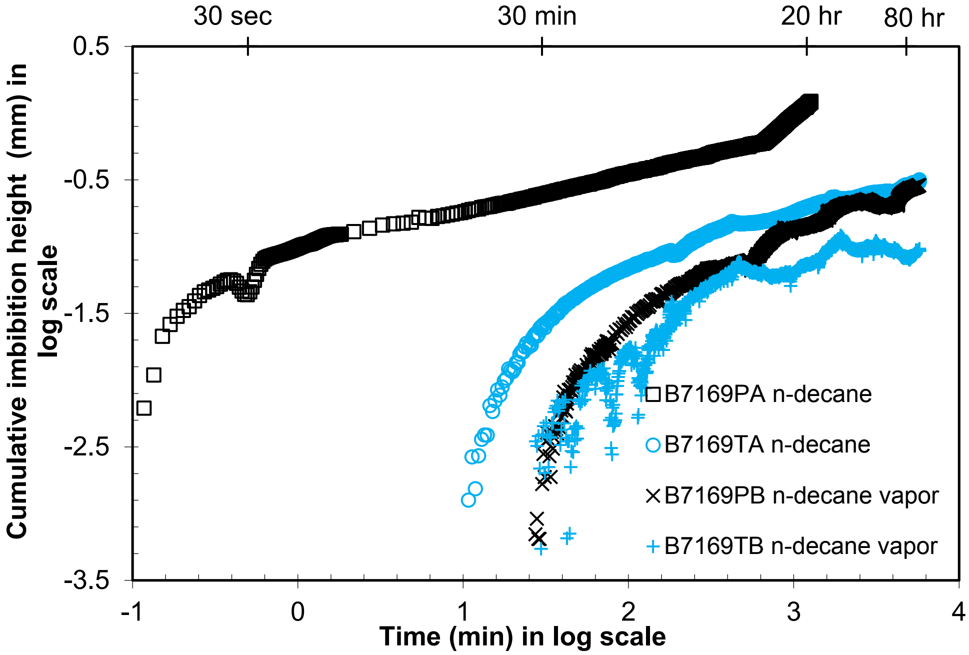

Figure 5-6 Cumulative n-decane Imbibition (mm) vs. Time (min) in Log Scales for B7169 Samples

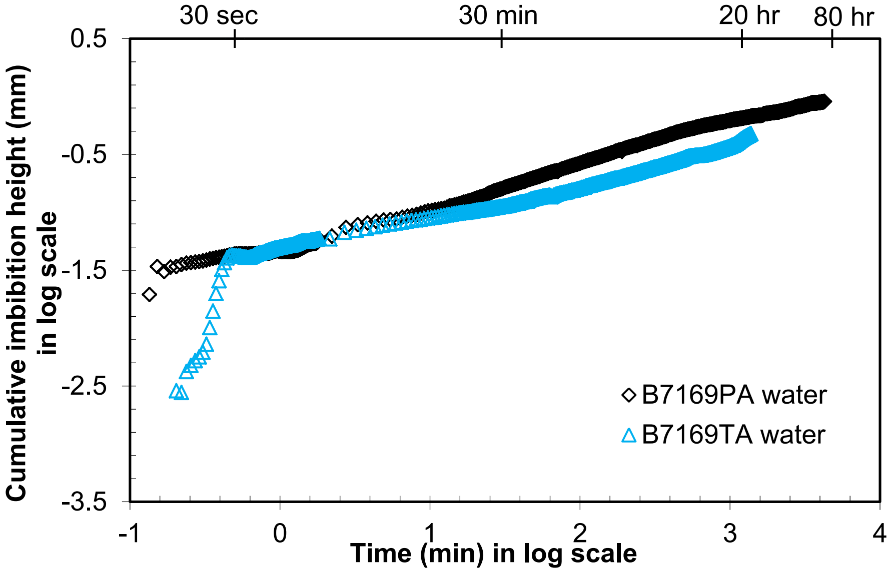

Figure 5-7 Cumulative Water imbibition (mm) vs. Time (min) in Log Scales for B7169 Samples

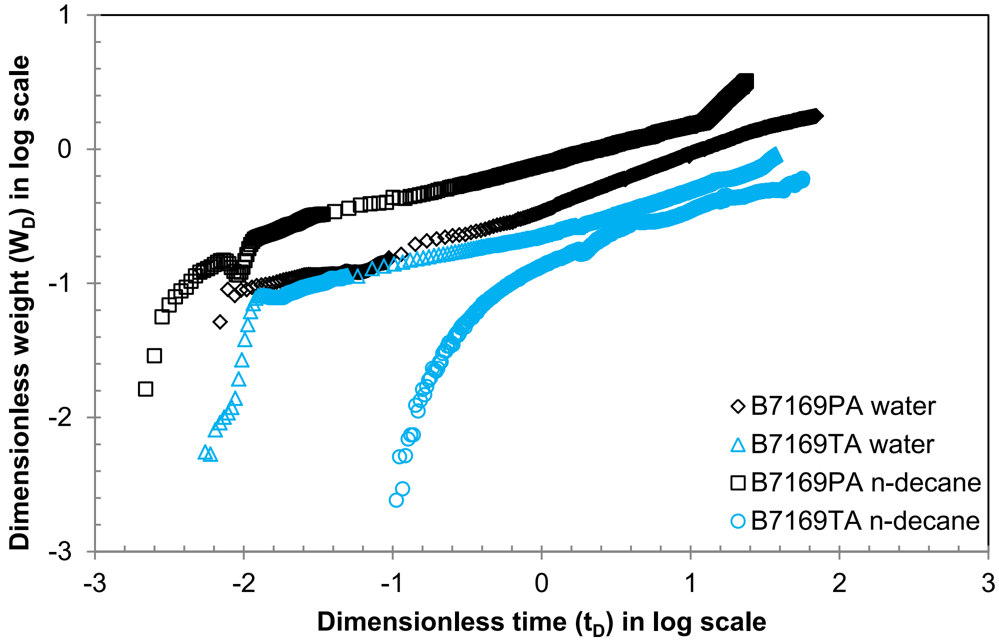

Figure 5-8 W_D vs t_D for B7169 Samples

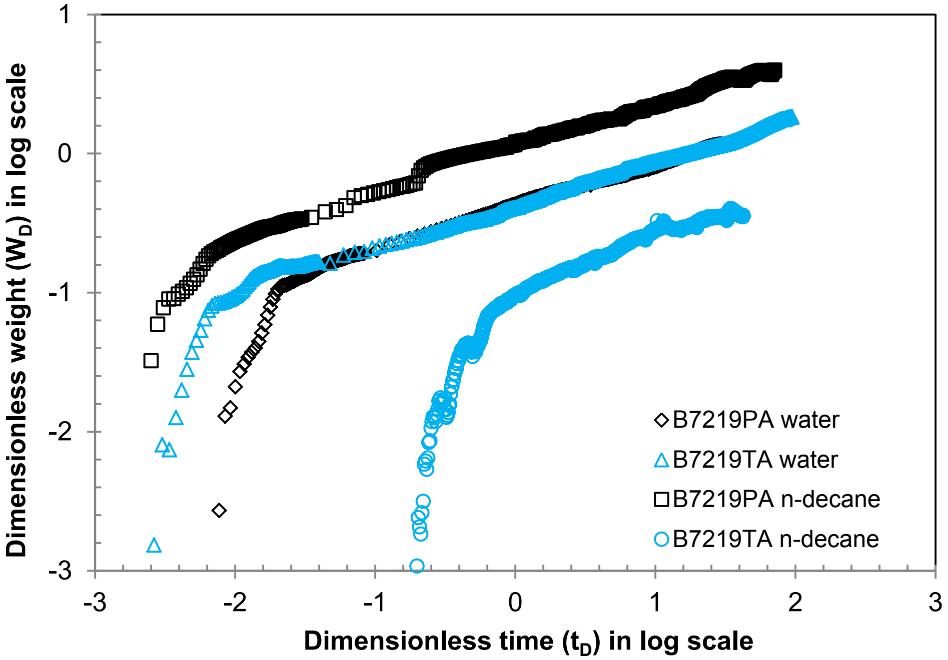

Figure 5-9 W_D vs t_D for B7219 Samples

5.4.1.3. Intermediate-wet Barnett shale from the depth of 7199 ft (B7199)

Unlike the oil-wet (B7136) or strongly water-wet samples (B7169 and B7219), B7199 samples showed some intermediate imbibition behavior (Figure 5-10). The water imbibition curves of B7199 P and T samples do not overlie one another closely and the P sample has a higher imbibition slope, indicating wetting characteristics different from those of strongly water-wet samples. In the n-decane experiments the P sample imbibed much more n-decane than the T sample during the early part of the experimental period, which is similar to the behavior observed for strongly water-wet samples; the difference between the two categories is that B7199 TB began to imbibe n-decane in a linear fashion at the very beginning of this experiment, in a pattern similar to that of oil-wet samples. The n-decane imbibition curve has a higher slope than the water imbibition curve for T samples which also indicates that B7199 is oil-wet to some extent. Based on these phenomena, B7199 is differentiated from other two wetting categories and considered as intermediate-wet.

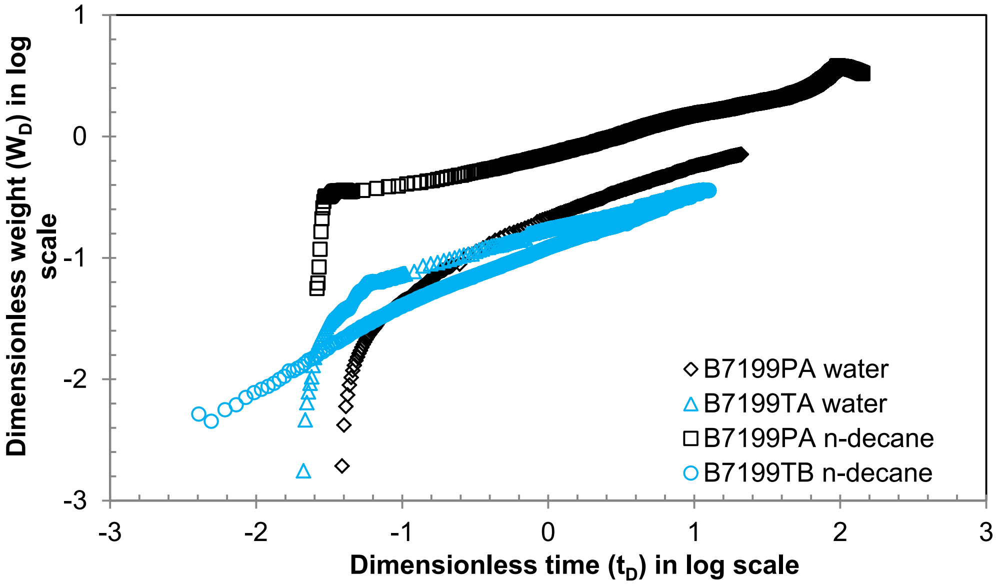

Figure 5-10 W_D vs t_D for B7199 Samples

5.4.2. Pore-throat Size Distribution of Barnett Shale

As a supplemental characterization method of SI experiments, MIP tests were performed on Barnett shale from the four different depths to obtain the pore-throat size distribution information; the results are shown in Figures 5-11 and 5-12. Hartmann and Beaumont [35] classified the pore sizes as nanopores (<0.1 μm), micropores (0.1-0.5 μm), mesopores (0.5-2.5 μm), macropores (2.5-10 μm) and megapores (>10 μm). Except for the B7136 sample, the dominant pore-throat sizes for the Barnett shale samples are less than 0.1 μm and fall in the nanopore range. Even for the B7136 sample, these nanopores account for about 20% of the total pore space.

The results shown in Figures 5-11 and 5-12 suggest that the samples fall into three groups in terms of their pore-throat size distribution, and that these three groups coincide with the three wettability categories defined on the basis of the SI experiments; this in turn indicates that some correlation may exist between pore structure and wettability. The oil-wet B7136 sample has the lowest porosity (~1%) and more than 25% of the total porosity is occupied by large pores (above 100 μm); the intermediate-wet B7199 sample has the highest porosity (~6%) and only about 4% of the pore spaces are occupied by large pores. The strongly water-wet B7169 and B7219 samples exhibit similar pore-throat size distributions which fall between those of the oil-wet and intermediate-wet samples.

5.4.3. Low Pore Connectivity of Barnett Shale

Pore connectivity plays an important role in fluid flow and mass transport in porous media; Hu et al. [40] investigated pore connectivity using multiple approaches, including water imbibition experiments. Unlike the conventional oil/gas reservoirs which likely have well-connected pore spaces, the pores of Barnett shale are poorly connected making the migration of fluids within them difficult.

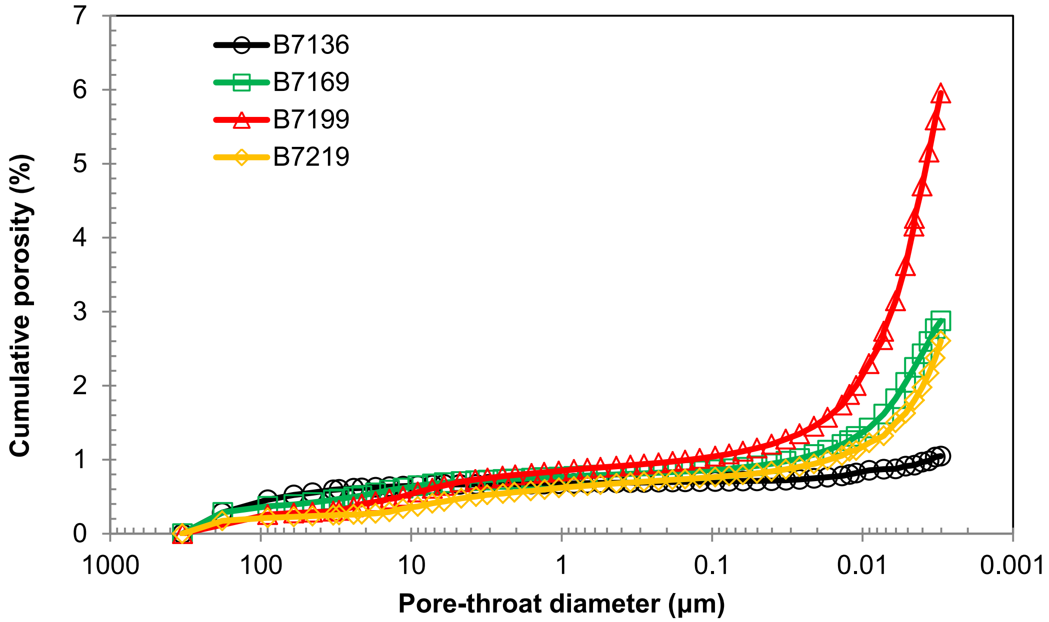

Figure 5-11 Cumulative Porosity vs. Pore-throat Diameter for Barnett Shale

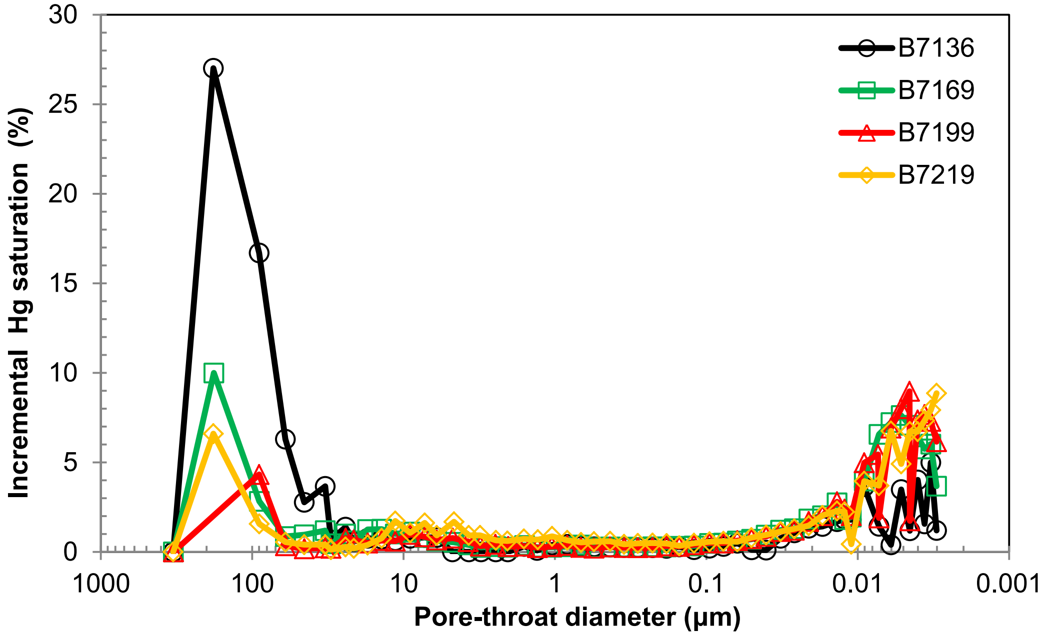

Figure 5-12 Incremental Hg Saturation vs. Pore-throat Diameter for Barnet Shale

If we plot cumulative water imbibition height versus imbibition time in log scales, the theoretical imbibition slope of 0.5 should be observed according to Handy's equation. However, our results (Table 5-3) show that the water imbibition slopes (around 0.28) of Barnett shale differ significantly from this theoretical 0.5 value. This confirms the low pore connectivity of Barnett shale [40].

Tortuosity which may be derived from MIP data according to Eq. (5-8) is another parameter that could be used to evaluate pore connectivity. The relatively large values of tortuosity (>10,000) shown in Table 5-3 implies fluids need to navigate through quite tortuous pathways in order to migrate from one location to another within the Barnett shale. This means that a fluid particle would have to travel more than 100 meters in order to traverse a core one centimeter in length, or in order to advance a linear distance of one centimeter in the formation. We believe that the nanopores of Barnett shales are very poorly connected so that fluids waste lots of time to connected pathways of limited distance.

Table 5-3 Water Imbibition Slopes and Tortuosities for Barnett Shale

Sample	Permeability (m^2)[a]	Tortuosity[b]	water imbibition slope[c,d]
B7136	1.14E-21	40603	0.269±0.005
B7169	2.21E-21	27795	0.273±0.050
B7199	4.96E-21	10352	0.284±0.062
B7219	1.78E-21	23591	0.313±0.019

[a] Permeability calculated according to KT method [42, 43].

[b] Tortuosity calculated according to Eq. (5-8) [33, 87].

[c] Only T samples are used to eliminate the effect of cracks within samples.

[d] Average±standard deviation for at least triplicate measurements on the same sample.

5.5 Conclusion

The goal of this work was to investigate Barnett shale samples from four depths (7136, 7169, 7199, and 7219 ft) using SI experimentation and MIP. We proposed a method to investigate the wettability characteristics of these layered shale samples by conducting imbibition experiments, in directions both parallel to (P) and transverse to (T) the bedding, using two types of imbibing fluids. Based on the SI results, the following wettability categories were qualitatively identified: (1) oil-wet B7136 samples; (2) strongly water-wet B7169 and B7219 samples; and (3) intermediate-wet B7199 samples. It should be noted that the directional dependency of imbibition was also used to differentiate these three wettability categories. For oil-wet samples, the slopes of n-decane imbibition were higher than those of water imbibition for both P and T samples, and there was no obvious n-decane imbibition difference between P and T samples. However, for strongly water-wet samples, the P and T experiments showed quite different n-decane imbibition behavior, whereas similar water imbibtion behavior was observed in the two directions, as would be expected for this category. Because of the strong water–wet condition, the transport of n-decane across bedding planes was inhibited, while in the direction parallel to these layers n-decane was apparently able to migrate along cracks created naturally or artificially among these layers. For intermediate-wet samples, the difference between P and T samples was observed in both water and n-decane imbibition curves. These three wettability categories also showed different pore-throat size distributions, which indicates the pore structure may affect wettability in some way. However, the relationship between pore structure and wettability is currently not clear and needs to be investigated in the future.

The low pore connectivity of Barnett shale, probably associated with low porosities and nanopores, was indicated by both the water imbibition slopes (around 0.28

as opposed to the theoretical slope of 0.5) and the high tortuosity values derived from MIP data.

Chapter 6

Experimental Studies of Spontaneous Imbibition, Median Pore-throat Diameter, and Wettability

6.1 Abstract

Spontaneous imbibition (SI) has been investigated by many researchers because of its significance in understanding the process of oil/gas recovery. However, most of current studies focus on evaluating the performance of the proposed scaling method on the same type of rock, and the pore structure information is insufficiently considered in these scaling methods. This work investigates the effect of median pore-throat diameter (D_{50}) on SI process for different porous media (Barnett shale, dolomite and Indiana sandstone). Parameter D_{50} is defined as the pore-throat diameter corresponding to 50% mercury saturation during mercury intrusion porosimetry measurement. The effect of D_{50} on wettability by changing the contact angle between imbibing fluid and porous medium is also investigated in this work using water and n-decane. Our results show that these three types of rocks tend to be more oil-wet and less water-wet as the increase of D_{50}. The imbibition curves of these three types of rocks are better correlated after D_{50} is taken into account, compared with scaled SI data without considering D_{50}. This also indicates that D_{50} as an index of pore structure plays an important role in the process of SI.

6.2 Introduction

Spontaneous imbibition (SI) is a capillary-force controlled process during which a wetting fluid displaces the non-wetting fluid by capillary force only, and it plays an important role in gas/oil recovery of fractured reservoirs. The properties of displacing and displaced fluids, pore structure of porous media and their interactions are the main factors controlling the imbibition process. Scaling of SI data is a good method to investigate the factors affecting imbibition process, and this approach is widely used to predict the gas/oil production behavior in the field with laboratory imbibition tests. Mattax and Kyte [58] proposed the following classical scaling equation,

$$t_D = t\sqrt{\frac{k}{\emptyset}}\frac{\sigma}{\mu_w L^2} \tag{6-1}$$

where t_D is dimensionless time; t is imbibition time (s); k is absolute permeability (m^2); $\emptyset$ is fractional pososity; σ is interfacial tension (N/m) between wetting and non-wetting phases; μ_w is viscosity of imbibing water (Pa·s); L is length (m).

Much effort has been spent on improving the performance of this scaling equation. After two major revisions made by Zhang et al. [90] and Ma et al. [55], a new definition of dimensionless time is proposed as Eq. (6-2),

$$t_D = t\sqrt{\frac{k}{\emptyset}}\frac{\sigma}{\sqrt{\mu_{we}\mu_{nw}}L_c^2} \tag{6-2}$$

where μ_{we} is the viscosity of wetting phase (Pa·s); μ_{nw} is the viscosity of non-wetting phase (Pa·s); L_c is characteristic length (m) which is defined by Eq. (6-3),

$$L_c = \sqrt{\frac{V_b}{\sum_{i=1}^{n} A_i / l_{A_i}}} \tag{6-3}$$

where V_b is the bulk volume of the matrix (m^3);n is the total number of surfaces open to imbibition; A_i is the area open to imbibition in the ith direction (m^2); l_{A_i} is the distance that the imbibition front travels from the imbibition face to the non-flow boundary (m).

The use of geometrical mean of the fluid viscosities, proposed by Zhang et al. [90] to account for the variations in the viscosity of the displaced phase, is empirical without any theoretical basis. The assumptions for this dimensionless time are (1) wettability must be the same; (2) relative permeability functions must be identical; (3)

capillary pressure functions must be identically proportional to interfacial tension; (4) initial fluid distributions must be duplicated; (5) gravity must be neglected.

It should be pointed out that all the studies related to scaling method mentioned above have one thing in common: they performed the scaling method on the same type of rock-fluid system and in this situation all the assumptions for Eq. (6-2) could be satisfied. However, Eq. (6-2) does not work well when it is applied to different types of rocks because the assumptions (1) and (3) are probably not the case due to the effects of pore structure. Akin et al. [2] conducted a research to investigate the SI characteristics of diatomite and they made a comparison between Berea sandstone and diatomite by scaling the SI data of these two types of rocks using Eq. (6-2). The scaled imbibition curves could not overlap with each other very well by showing a considerable difference: these diatomite samples imbibed water at rates that rival sandstone in an absolute sense and exceeded sandstone in a non-dimensional sense although diatomite is 100 times less permeable that sandstone. The authors concluded that this difference was due to capillary force, but no further investigation was performed.

Recently, some researches have been conducted to provide scaling groups that are independent of fluid and rock properties [9, 73], and the validity of these proposed methods has been demonstrated. However, the effect of pore structure on fluid transport in porous media is not considered in these studies. Here we will investigate the effect of pore structure on imbibition process. The median pore-throat diameter (D_{50}), as an important index of pore structure, has attracted many researchers' attention [28, 65, 69]. Gao and Hu [28] proposed an empirical equation to estimate permeability solely using D_{50}, which indicated the importance of D_{50} in controlling fluid transport in porous media. This work is the first time to investigate the effect of D_{50} on SI process and the theoretical background will be provided in the Theory section.

Mercury intrusion porosimetry (MIP) has been widely used to characterize the pore-throat size distribution for several decades, since Washburn [86] proposed the basic theory as follows,

$$\Delta P = -\frac{2\gamma cos\theta}{R} \tag{6-4}$$

where ΔP is the pressure difference across the curved mercury interface (dyne/cm^2); γ is the surface tension of mercury (485 dynes/cm); θ is the contact angle (130°) between mercury and the porous media; R is the corresponding pore-throat radius (cm).

Besides pore-throat size distribution, several parameters (such as permeability, tortuosity, and fractal dimension) could be derived from MIP data [26, 33, 42, 43, 82]. Although some issues related to its application like hysteresis phenomenon and contact angle changes are discussed in the literature [20, 23, 60, 92], MIP is still considered as a powerful characterization tool because of its simple principle and wide coverage of pore sizes (usually from 10^{-9} to 10^{-4} m) [46].

6.3 Theory

Handy [34] proposed a classical equation (Eq. (6-5)) to describe the SI process in water-air system during which imbibition occurs vertically upward,

$$Q_w = at^{0.5} \tag{6-5}$$

where

$$a = \left(\frac{2P_c k_w \emptyset A^2 S_w}{\mu_w}\right)^{0.5} \tag{6-6}$$

Q_w is the volume of water imbibed into the core sample; a is a constant; P_c is the capillary pressure; k_w is the effective permeability; $\emptyset$ is fractional porosity; A is the cross-section area of the core; S_w is fractional water content of the pore spaces; t is imbibition time; μ_w is viscosity of water. From Handy's equation, we can observe that the weight or volume of the imbibed water is proportional to the square root of the imbibition time and the slope *a* depends on the parameters within parenthesis in Eq. (6-6).

After the introduction of t_D, defined by Eq. (6-2), and dimensionless weight (W_D), Eq. (6-5) could be simply rewritten as

$$W_D = bt_D^{0.5} \tag{6-7}$$

where

$$W_D = W/[\rho \emptyset V] \tag{6-8}$$

W_D is the dimensionless weight; *b* is a constant; *W* is the imbibed weight of fluid (water or *n*-decane); ρ is the density of water or *n*-decane; $\emptyset$ is fractional porosity; *V* is sample volume.

For the same type of porous medium, the slope *b* should remain the same if all the assumptions (listed in Section 6.2) are satisfied. However, the assumptions about wettability and capillary pressure for Eq. (6-2) are not appropriate for different porous media. The relationship between capillary pressure and interfacial tension is described by Young-Laplace Law as shown in Eq. (6-9),

$$P_c = P_g - P_l = \frac{2\sigma cos\theta}{r} \tag{6-9}$$

where P_c is capillary pressure; P_g is the pressure in the gas phase; P_l is the pressure in the liquid phase;σ is interfacial tension between gas and liquid phases; θ is contact angle in the liquid phase; *r* is pore radius.

Therefore, not only the interfacial tension, but also contact angle and pore sizes, determine the capillary pressure. Different contact angles and pore sizes are always expected for different porous media and no evidence exists that the ratio of $cos\theta/r$ is identical for different porous media. Based on Eqs. (6-5) to (6-9), the following relationship could be derived,

$$b \propto \left(\frac{cos\theta}{d}\right)^{0.5} \tag{6-10}$$

where *d* is pore diameter.

By the definition of wettability, we know that it depends on the contact angle θ and the effect of wettability could be covered by the ratio of $cos\theta/d$. If contact angle θ is constant for different porous media, slope *b* should be inversely proportional to the square root of pore diameter *d*. However, contact angle may be different for different porous media, and even for the same porous medium contact angle may vary if different fluids are used in imbibition experiment. In this work, we will use D_{50} obtained from MIP as the representative pore diameter for porous media to investigate the relationship between slope *b* and D_{50}, and compare the derived relationship with the theoretical relationship (Eq. (6-10)) to assess the effects of D_{50} on contact angle.

6.4 Experiments

We perform imbibition experiments and MIP tests on Barnett shale, dolomite and Indiana sandstone. These three types of rocks have quite different pore sizes, which makes our results more representative. Among these samples, Barnett shale is the tightest one and Indiana sandstone has the largest pore sizes while the pore sizes of dolomite fall between the other two rocks.

The SI apparatus has been shown by Gao and Hu [27] and the detailed experimental procedure and data processing method are provided by Hu et al. [39]. During SI experiments, all sides of sample (in the shape of prism) were coated with quick-cure epoxy except top and bottom to make a co-current imbibition in vertical direction. All the samples were oven-dried at 60 ºC for at least 48 hours before going through SI experiments in order to get a constant initial water saturation state. Water and n-decane were selected as the imbibing phase during imbibition experiments to displace air. The dimensions of samples used in imbibition experiments and other important parameters are shown in Table 6-1.

The density of water is 1.00 g/cm^3, viscosity of water is 1.002 mPa•s, the interfacial tension of water with air is 72.0 mN/m; the density of n-decane is 0.73 g/cm^3, viscosity of n-decane is 0.84 mPa•s, the interfacial tension of n-decane with air is 23.9 mN/m; the viscosity of air is 0.018 mPa•s.

Micromeritics AutoPore IV 9510 is the instrument we used to perform MIP tests on the three types of rocks. The highest pressure it could generate during high-pressure analysis is 60,000 psia (413MPa) and the correspondingly intruded pore-throat diameter is about 3.0 nm, while the largest pore-throat diameter measurable by MIP during low-pressure analysis is about 300 microns. All the samples were oven-dried at 60 ºC for at least 48 hours to remove moisture in the pore spaces and then cooled to room temperature (~23 ºC) in a desiccator before they went through the MIP test.

Table 6-1 The Properties of Samples Used in SI Experiments

Sample	Porosity[a]	Permeability[a] (m^2)	sample ID	Fluid used	Length (cm)	Width (cm)	Height (cm)
Barnett shale	0.060	4.96E-21	B1	water	1.2	1.7	1.7
			B2	n-decane	1.7	1.3	3.9
Dolomite	0.091	9.80E-17	D1	water	1.5	1.5	1.5
			D2	n-decane	1.5	1.5	1.5
Indiana sandstone	0.167	1.80E-13	I1	water	1.5	1.5	1.5
			I2	n-decane	1.5	1.5	1.5

[a] From Gao and Hu [28].

6.5 Results and Discussion

6.5.1. Pore-throat Size Distribution

Pore-throat size distribution obtained by MIP for our samples is shown in Figure 6-1 and these three types of rocks show quite different pore-throat size distribution. Indiana sandstone has the largest pore-throat sizes and most of the pore-throat sizes are above 10 μm, while the dominant pore-throat sizes of Barnett shale are less than 0.01 μm. Unlike Barnett shale and Berea sandstone with a relatively narrow pore-throat size range indicated by their steep slopes in Figure 6-1, dolomite possesses a wider pore-throat sizes that are mainly distributed in the range of 0.01-10 μm. The D_{50}, defined as the pore-throat diameter corresponding to 50% mercury (Hg) saturation, is also indicated in Figure 6-1; the D_{50} values for Barnett shale, dolomite and Indiana sandstone are 0.0065 μm, 0.873 μm and 17.9 μm, respectively.

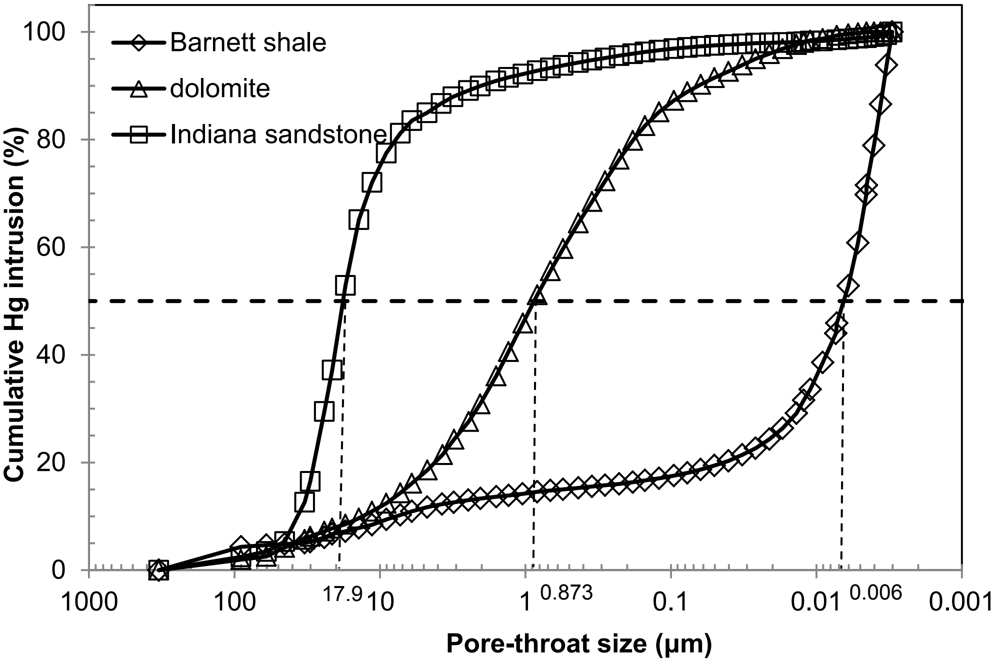

Figure 6-1 Cumulative Hg Intrusion (%) vs. Pore-throat Size (μm)

6.5.2. Relationship between the Slope b in Eq. (6-7) and D_{50} and the Effect of D_{50} on Wettability

We will discuss individual water and n-decane imbibition behaviors for the three types of rocks.

As described by Eq. (6-7), a linear relationship should exist between W_D and the square root of t_D, and the results of scaled water imbibition using Eq.(6-2) are shown in Figure 6-2. It is obvious that the three water imbibition curves were not well correlated by using t_D defined by Eq. (6-2), and a D_{50} relevant behavior was observed as supposed by Eq. (6-10). Barnett shale with the smallest D_{50} showed a quite high water imbibition potential in an absolute sense, while Indiana sandstone with the largest D_{50} exhibited the lowest imbibition slope in these three rock types. For n-decane imbibition, similar results are presented in Figure 6-3 and the plateau area found for both dolomite and Indiana sandstone imbibition curves is due to the arrival of n-decane at the top sample surface.

If we compare the scaled water imbibition curve in Figure 6-2 with n-decane imbibition curve in Figure 6-3 for the same type of rock, wettability could be indicated from the slope difference because all the factors affecting SI process except wettability have been compensated in this case by using t_D defined by Eq. (6-2). Barnett shale with the smallest D_{50} has an intermediate wettability because of its similar water and n-decane imbibition slopes. Indiana sandstone with largest D_{50} is strongly oil-wet due to its large difference between water and n-decane imbibition slopes (the slope of n-decane imbibition is almost 30 times higher than that of water imbibition). Furthermore, dolomite tends to be oil-wet according to its higher slope of n-decane imbibition compared with water imbibition. Basically these three types of rocks tend to become more oil-wet as the increase of D_{50}.

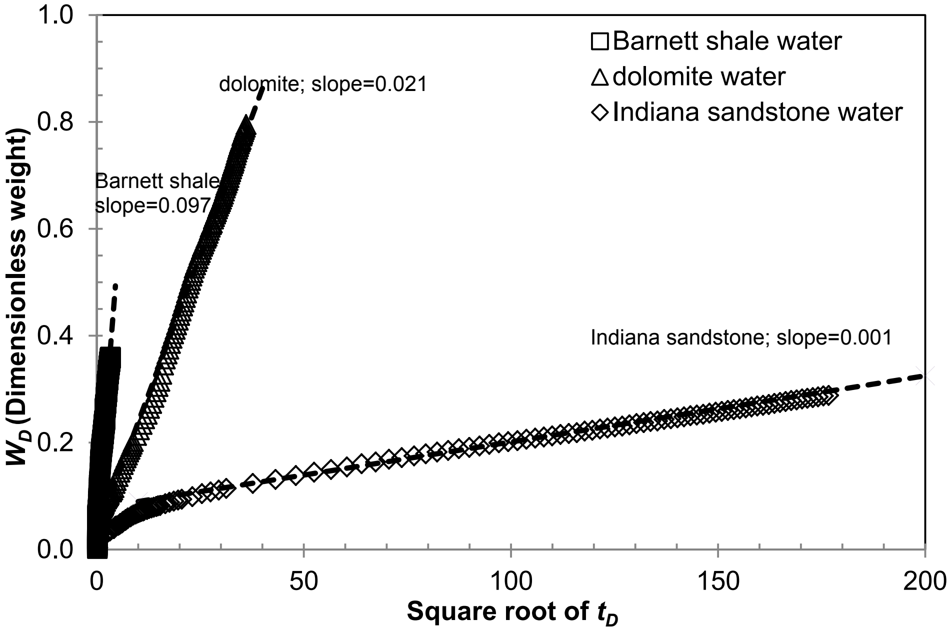

Figure 6-2 W_D (dimensionless weight) vs. Square Root of t_D (dimensionless time), Water-air Imbibition

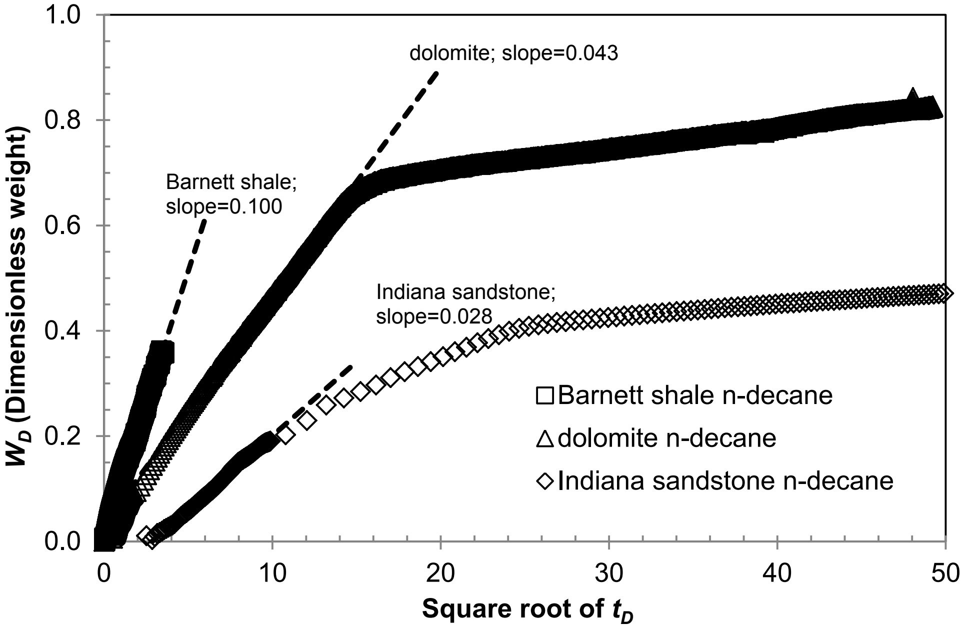

Figure 6-3 W_D (dimensionless weight) vs. Square Root of t_D (dimensionless time), n-decane-air ImbibitioN

After plotting slope *b* versus D_{50} in Figure 6-4, an exponential correlation was found for both water and n-decane imbibition.

For water-air-rock system, the following relationship exists,

$$b = 0.0091 \times D_{50}^{-0.528} \tag{6-11}$$

where *b* is the slope defined by Eq. (6-7); D_{50} is the median pore-throat diameter in μm.

For n-decane-air-rock system, the exponential relationship is

$$b = 0.0438 \times D_{50}^{-0.161} \tag{6-12}$$

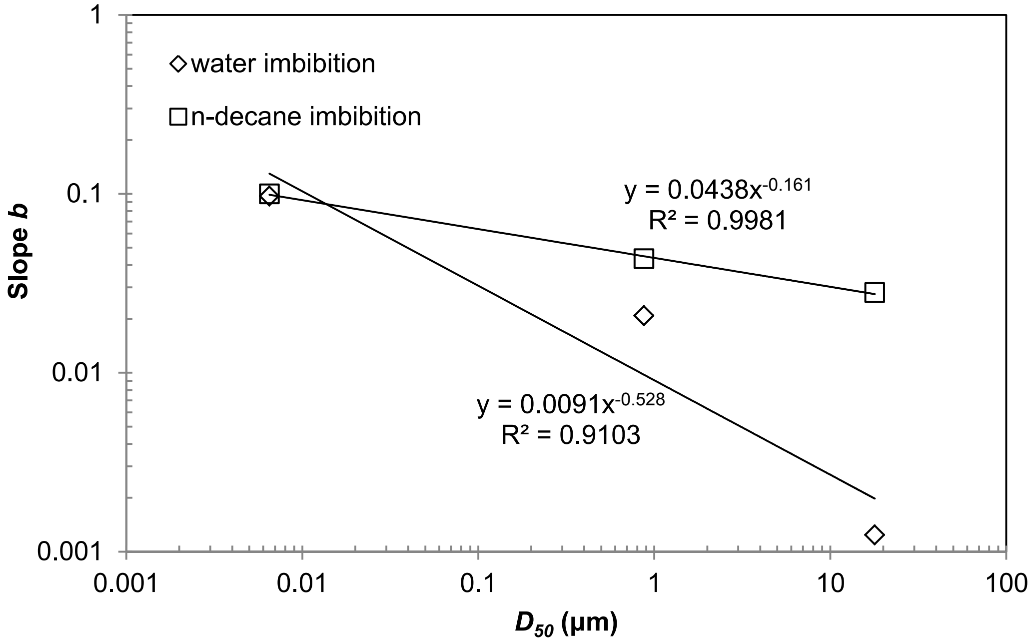

Figure 6-4 Slope *b* vs. D_{50}

An exponent of -0.5 should exist between *b* and D_{50} if contact angle remains the same according to Eq. (6-10); this is not supported by our results. Especially for the n-decane-air-rock system, an exponent of -0.161 (R^2=0.9981) was obtained which indicates the contact angle between n-decane and rock is significantly affected by D_{50}.

A combination of Eq. (6-12) and Eq. (6-10) could give us the following relationship between contact angle and D_{50} for n-decane-air-rock system,

$$cos\theta_d \propto D_{50}^{0.678} \tag{6-13}$$

where θ_d is the contact angle between n-decane and porous medium.

For water-air-rock system, an exponent of -0.528 (R^2=0.9103) is derived between slope *b* and D_{50}, which deviates a little from the expected exponent of -0.5. Although not like n-decane imbibition which shows obvious deviation, this small deviation for water imbibition also indicates D_{50} could affect contact angle between water and rock to a small extent.

An opposite relationship for water-air-rock system was derived between contact angle and D_{50} compared with n-decane-air-rock system, when we combined Eq. (6-11) and Eq. (6-10),

$$cos\theta_w \propto \ D_{50}^{-0.056} \tag{6-14}$$

where θ_w is the contact angle between water and porous medium.

The less the value of θ_w, the more water-wet is the porous medium. Similarly, the less the value of θ_d, the more oil-wet is the porous medium. According to Eqs. (6-13) and (6-14), the porous medium becomes more oil-wet and less water-wet as the increase of D_{50}, which agrees with the wettability conditions of these three types of rocks discussed above by directly comparing scaled imbibition curves.

6.5.3. Scaling of SI Data Using D_{50}

Based on Eqs. (6-7), (6-11) and (6-12), D_{50} is introduced to the dimensionless time t_D separately for water and n-decane imbibition. For water imbibition, the new dimensionless time $t_{D\text{-}new\text{-}w}$ is derived as follows,

$$t_{D-new-w} = (D_{50}^{-1.056}) \times t_D \qquad (6\text{-}15)$$

where D_{50} is in μm; t_D is defined by Eq. (6-2).

For n-decane imbibition, the new dimensionless time $t_{D\text{-}new\text{-}d}$ is

$$t_{D-new-d} = (D_{50}^{-0.322}) \times t_D \qquad (6\text{-}16)$$

The results of scaled imbibition data using new dimensionless time for water and n-decane are shown in Figures 6-5 and 6-6, respectively. Although the water imbibition curve of dolomite deviates a little bit from other two curves after using $t_{D\text{-}new\text{-}w}$, they indeed become much closer to each other than using t_D without D_{50}. The advantage of using new dimensionless time is more obvious for n-decane imbibition, the imbibition curves are well correlated for these three types of rocks after D_{50} is taken into account (Figure 6-6).

It should be noted that these proposed scaling equations depend on the fluids used in SI experiments, which means Eq. (6-15) is only applicable to water-air-rock system, while Eq. (6-16) could be used to predict the imbibition behavior of n-decane-air-rock system. Although many studies have been conducted to investigate the spontaneous imbibition, very few of them paid attention to the effect of D_{50} on imbibition. This work is the first time to investigate the effect of D_{50} on spontaneous imbibition and to propose the scaling equation using D_{50}.

Schmid and Geiger [73] proposed the universal scaling of spontaneous imbibition for water-wet systems, and the following equation was used during derivation,

$$Q_W(t) = 2At^{1/2} \qquad (6\text{-}17)$$

where $Q_w(t)$ is the imbibed distance (m); A is a parameter which depends on the characteristics of the fluid-rock system (m/$\sqrt{s}$); t is imbibition time (s).

They selected many published imbibition datasets to verify the proposed scaling method, and nearly all of these datasets used water-oil-rock system. However, the dataset from Babadagli and Hatiboglu [7] used water-air-rock system and Berea sandstone was the rock they investigated, and we will use this dataset to verify Eqs. (6-11) and (6-15).

The following relationship could be obtained after combining Eqs. (6-1)–(6-3), (6-5)–(6-8), and (6-17),

$$b = \frac{2A}{\left(\sqrt{\frac{k}{\emptyset}}\frac{\sigma}{\sqrt{\mu_{we}\mu_{nw}}}\right)^{0.5}} \tag{6-18}$$

As a result, if all the parameters in the right side of Eq. (6-18) are known, we could calculate the slope *b* and then estimate *D*$_{50}$ according to Eq. (6-11).

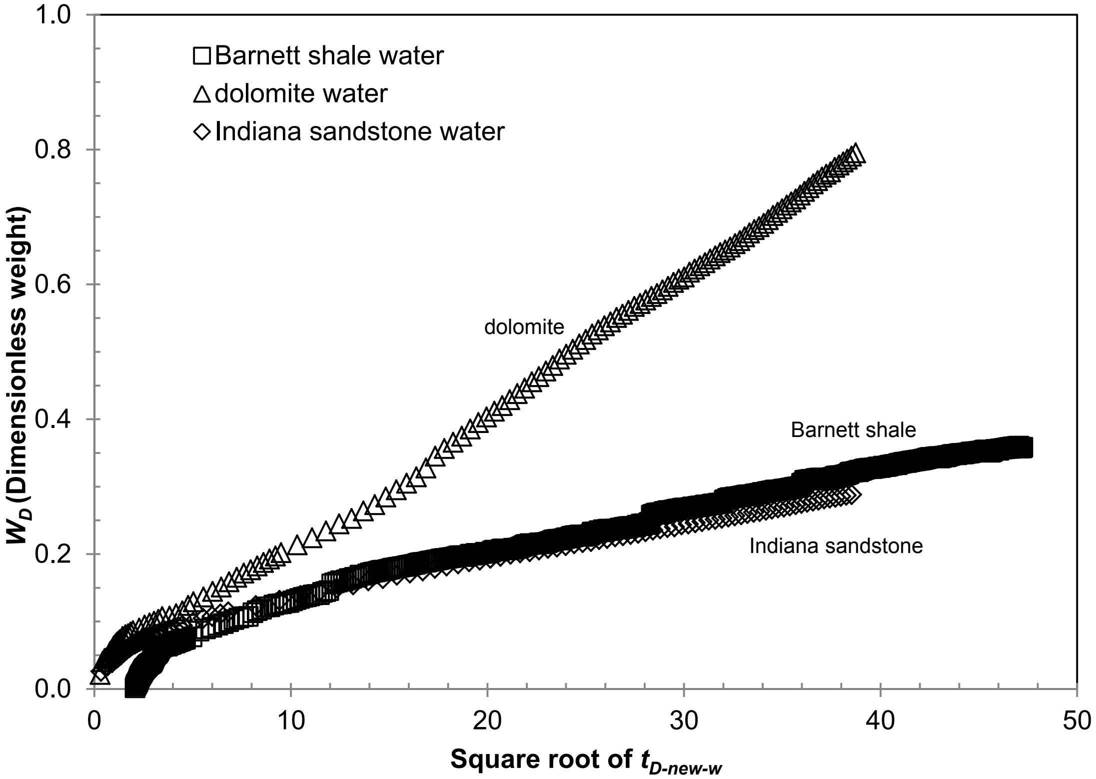

Figure 6-5 W_D (dimensionless weight) vs. Square Root of $t_{D\text{-}new\text{-}w}$ (new dimensionless time for water imbibition)

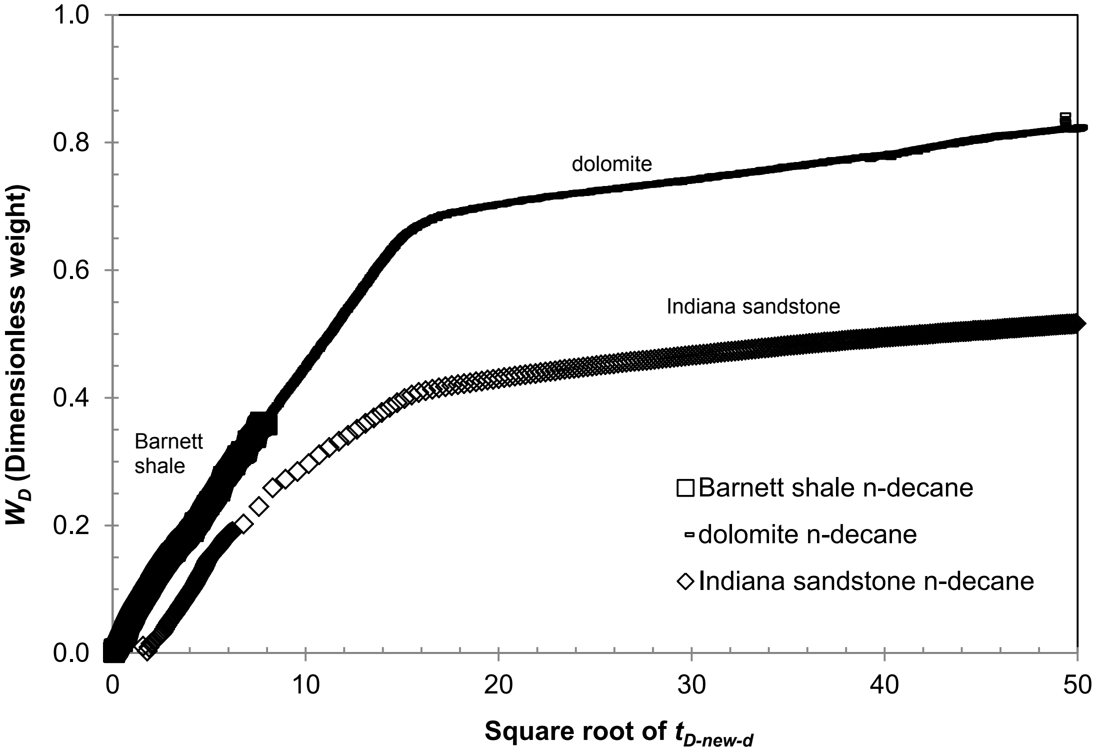

Figure 6-6 W_D (dimensionless weight) vs. Square Root of $t_{D\text{-}new\text{-}d}$ (new dimensionless time for n-decane imbibition)

The calculated slope *b* and D_{50} together with other parameters from the dataset of Babadagli and Hatiboglu [7] are shown in Table 6-2. The average value of calculated D_{50} was quite near the measured D_{50} value, which somewhat verify the applicability of Eqs. (6-11) and (6-15) on water-air-Berea sandstone system.

Table 6-2 Calculated Slope b and D_{50} for Berea Sandstone

A[a] (m/s$^{0.5}$)	Porosity[b]	k[b] (m^2)	σ[b] (N/m)	μ_{we}[b] (Pa·s)	μ_{nw}[b] (Pa·s)	b	Calculated D_{50}(μm)	Average D_{50} (μm) ± standard deviation	Measured D_{50}[c] (μm)
2.75E-05	0.21	5E-13	0.072	0.001	1.80E-05	0.0019	19.211	31.358 ±13.102	22.982
2.81E-05	0.21	5E-13	0.072	0.001	1.80E-05	0.0020	18.442		
1.95E-05	0.21	5E-13	0.072	0.001	1.80E-05	0.0014	36.839		
2.29E-05	0.21	5E-13	0.072	0.001	1.80E-05	0.0016	27.171		
1.60E-05	0.21	5E-13	0.072	0.001	1.80E-05	0.0011	53.583		
2.07E-05	0.21	5E-13	0.072	0.001	1.80E-05	0.0014	32.900		

[a] From Schmid and Geiger [73];
[b] From Babadagli and Hatiboglu [7];
[c] From Gao and Hu [28].

6.6 Conclusion

The objective of this work was to investigate the effect of D_{50} obtained from MIP on SI process. By analyzing the relationship between slope b in Eq. (6-7) and D_{50}, the influence of D_{50} on wettability by affecting the contact angle between imbibing fluid and porous medium was also investigated. The results showed that the three types of rocks used here tend to be more oil-wet and less water-wet from the observed increase of D_{50}, which could also be concluded by directly comparing water and n-decane imbibition curves. Different relationships were obtained between b and D_{50} for water and n-decane imbibition respectively, which also indicated the necessity of discussing water and n-decane imbibition separately. The classical scaling method without considering D_{50} could not correlate imbibition curves of different porous media very well, while the new proposed scaling methods using D_{50} (Eqs. (6-15) and (6-16)) showed better results, which indicated the importance of D_{50} in SI process.

The scaling equations proposed for water-air-rock systems were verified to be applicable on Berea sandstone by using imbibition data from Babadagli and Hatiboglu [7] while there was no data available in the literature to verify the equations proposed for n-decane-air-rock system. However, our results indeed showed the importance of D_{50}, which is an important index of pore structure, in controlling fluid transport in porous media.

It should be noted that the new scaling methods depend on fluids used during SI experiments, and they could be improved as more SI data are collected in the future. For different fluid-rock systems, different scaling equations considering D_{50} are expected. However, the derivation of these scaling equations for other fluid-rock systems requires a huge amount of work and is outside the scope of this paper with the focus of investigating the effect of pore structure (D_{50}) on SI process.

It also should be pointed out that all the samples were oven-dried under 60 ºC to get the same initial water saturation state ($S_{wi} \approx 0$) before going through SI experiments, so that the pore-throat size distribution obtained from MIP could reflect the pore structure of samples used in SI experiments because MIP could only test dried samples. The effect of different sample treatments (e.g. aging samples using different oil phases with different time lengths) on D_{50} is still unknown and needs to be investigated in the future.

Chapter 7

Conclusions

7.1 Permeability Calculation from Imbibition Tests

A new method has been proposed in Chapter 2 to derive the effective permeability of unsaturated building materials from imbibition tests. The new derived linear relationship between water imbibition rate and the reciprocal of air recovery is supported by the results of imbibition experiments. The values of permeability estimated using our method are in line with literature permeability results. This new method can be applied to materials with a relatively high porosity (e.g., >15%) and well-connected pore structure.

7.2 The Application of MIP in Derivation of Permeability and Gas Diffusivity

Chapter 3 presents a new equation which solely uses the median pore-throat radius to estimate the permeability of porous consolidated media. Compared with the existing relationships, our new equation has the simple form, high reliability and wide applicability. The effect of porosity on permeability may be negligible compared with the effect of median pore-throat radius. For consolidated porous materials (rocks) this work is the first to only relate permeability to median pore-throat radius without considering other parameters. The samples used here also have a wide range of permeability (10^3 mD to 10^{-6} mD), which makes our new method more applicable.

Chapter 4 was to derive gas diffusivity from MIP data and to investigate the correlation of diffusivity with permeability and porosity. Our results show that the consideration of Knudsen diffusion in many rocks is necessary. The effective diffusion coefficients (D_e) of three types of porous media (building materials, consolidated rocks and unconsolidated sediments) were calculated with established equations, using average pore diameter (d_a) and porosity ($\emptyset_a$). Our results are basically in accordance with the experimental values obtained from gas diffusion tests. Although the method used to calculate D_e in this work is only applicable to samples with porosity between 0.05 and 0.95, this method still has a wide applicability (except for extremely tight rocks such as granite). Diffusivity was also used to obtain the m (cementation factor) value, which is closely related to the pore structure. And two groups of samples were divided according to the m values (m=1.5 vs. m=2.5).

7.3 Wettability of Barnett Shale Indicated from Directional Spontaneous Imbibition (SI) Tests

In Chapter 5 we proposed a method to qualitatively characterize the wettability information of these layered shale samples by conducting imbibition experiments, in directions both parallel to (P) and transverse to (T) the bedding, using two types of imbibing fluids (water/n-decane). As a result, three wettability categories were identified: (1) oil-wet B7136 samples; (2) strongly water-wet B7169 and B7219 samples; and (3) intermediate-wet B7199 samples. These three wettability categories also showed different pore-throat size distributions, which indicates the pore structure may affect wettability in some way.

The low pore connectivity of Barnett shale, probably associated with low porosities and nanopores, was confirmed by the lower water imbibition slopes (around 0.28 as opposed to the theoretical slope of 0.5) and the high tortuosity values calculated from MIP data.

7.4 The Effect of Median Pore-throat Diameter (d_{50}) on Fluid Migration in Porous Media

Diffusion and advection are two important processes controlling mass transport in porous media, while median pore-throat diameter plays an important role in both of these two forms of fluid migration.

As mentioned in Chapter 4, two groups of samples were divided according to the m values (m=1.5 vs. m=2.5). For the consolidated samples, these two groups could be further differentiated from each other according to d_{50} obtained from MIP. When d_{50} is larger than ~0.5 μm, the samples belong to the group with m=1.5. Conversely, if d_{50} is less than ~0.5 μm the sample probably has an m value of 2.5 and the samples in this group exhibit a more organized behavior and display an exponential relationship between gas diffusivity (D') and d_{50} as shown in Figure 4-5. All of these indicate the importance of d_{50} in gas diffusion process.

The sole use of median pore-throat radius (r_{50}) to predict permeability in Chapter 3 indicates that r_{50} may control the fluid flow in porous media. Furthermore, Chapter 6 investigated the effect of d_{50} on SI process. The influence of d_{50} on wettability by affecting the contact angle between imbibing fluid and porous medium was also investigated. Our results showed that the three types of rocks tend to be more oil-wet and less water-wet from the observed increase of d_{50}. The classical scaling method without considering d_{50} could not correlate imbibition curves of different porous media very well, while the new proposed scaling methods using d_{50} showed better results, which indicated the importance of d_{50} in SI process.

Appendix A

Publication Information of Chapters 2-6

Chapter 2: A manuscript published in Special Topics & Reviews in Porous Media. Zhiye Gao and Qinhong Hu, 2012, 3(3), 209-213.   .

Chapter 3: A manuscript published in Journal of Geophysics and Engineering. Zhiye Gao and Qinhong Hu, 2013, 10(2), 025014.

Chapter 4: A manuscript published in Journal of Porous Media. Zhiye Gao, Qinhong Hu and Hecheng Liang, 2013, 16 (7), 607-617.

Chapter 5: A manuscript submitted to Journal of Petroleum Science and Engineering. Zhiye Gao and Qinhong Hu.

Chapter 6: A manuscript submitted to Journal of Petroleum Science and Engineering. Zhiye Gao and Qinhong Hu.

References

[1] Adler, P. M., C.G. Jacquin, and J. F. Thovert. 1992. The formation factor of reconstructed porous media. *Water Resour. Res.,* 28(6): 1571–1576.

[2] Akin, S., J.M. Schembre, S.K. Bhat, and A.R. Kovscek. 2000. Spontaneous imbibition characteristics of diatomite. *J. Petrol. Sci. Eng.,* 25: 149–165.

[3] American Petroleum Institute Recommended Practice (API RP) 40. 1998. Recommended Practice for Core Analysis Procedure (2nd Ed.) (Washington, DC Am. Petrol. Inst.)

[4] Amott, E. 1959. Observations relating to the wettability of porous rock. *Trans. AIME.,* 216: 156–162.

[5] Annual Energy Outlook. 2012. National Energy Modeling System, run REF2012.D121011B.

[6] Archie, G.E. 1942. The electrical resistivity log as an aid in determining some reservoir characteristics. *Trans. AIME*., 146: 54–62.

[7] Babadagli, T. and C.U. Hatiboglu. 2007. Analysis of counter-current gas–water capillary imbibition transfer at different temperatures. *J. Petrol. Sci. Eng.,* 55 (3–4): 277–293.

[8] Bentz, D.P., D.A. Quenard, H.M. Kunzel, J. Baruchel, F. Peyrin, N.S. Martys, and E.J. Garboczi. 2000. Microstructure and transport properties of porous building materials. II. Three-dimensional X-tomographic studies. *Mater. Struc.,* 33: 147–153.

[9] Bjørnarå, T.I. and S.A. Mathias. 2013. A pseudospectral approach to the McWhorter and Sunada equation for two-phase flow in porous media with capillary pressure. *Comput. Geosci.,* DOI 10.1007/s10596-013-9360-4.

[10] Boving, T.B. and P. Grathwohl. 2001. Tracer diffusion coefficients in sedimentary rocks: correlation to porosity and hydraulic conductivity. *J. Contam. Hydrol.,* 53(1–2): 85–100.

[11] Bowker, K.A. 2007. Barnett Shale gas production, Fort Worth Basin: Issues and discussion. A*m. Assoc. Pet. Geol. Bull.,* 91(4): 523–533.

[12] Busch, A., S. Alles, Y. Gensterblum, and D. Prinz. 2008. Carbon dioxide storage potential of shales. *Int. J. Greenhouse Gas Control,* 2: 297–308.

[13] Carniglia, S.C. 1986. Construction of the tortuosity factor from porosimetry. *J. Catal.,* 102: 401–418.

[14] Chalmers, G.R., R.M. Bustin, and I.M. Power. 2012. Characterization of gas shale pore systems by porosimetry, pycnometry, surface area, and field emission scanning electron microscopy/transmission electron microscopy image analyses: Examples from the Barnett, Woodford, Haynesville, Marcellus, and Doig units. *Am. Assoc. Pet. Geol. Bull.,* 96(6): 1099–1119.

[15] Chilingar, G.V., R. Main, and A. Sinnokrot. 1963. Relationship between porosity, permeability, and surface areas of sediments. *J. Sediment. Petrol.,* 33(3): 759–765.

[16] Cui, X., A. Bustin, and R. Bustin. 2009. Measurements of gas permeability and diffusivity of tight reservoir rocks: Different approaches and their applications. *Geofluids,* 9: 208–223.

[17] Cunningham, R.E. and R.J.J. Williams. 1980. Diffusion in gases and porous media, Plenum, New York.

[18] Curtis, J.B. 2002. Fractured shale-gas systems*. Am. Assoc. Pet. Geol. Bull.,* 86(11): 1921–1938.

[19] Denekas, M.O., C.C. Mattax, and G.T. Davis. 1959. Effect of crude oil components on rock wettability. *Trans. AIME.,* 216: 330–333.

[20] Diamond, S. 2000. Mercury porosimetry: An inappropriate method for the measurement of pore size distributions in cement-based materials. *Cem. Concr. Res.,* 30: 1517–1525.

[21] Donaldson, E.C., R.D. Thomas, and P.B. Lorenz. 1969. Wettability determination and its effect on recovery efficiency. *SPE J.,* 9(1): 13–20.

[22] Du, J.K., J. Bao, Q.H. Hu, and R.P. Ewing. 2012. Uranium release from different size fractions of sediments in Hanford 300 Area, Washington, USA. *J. Environ. Radioact.,* 107: 92–94.

[23] EL-Dieb, A.S. and R.D. Hooton. 1994. Evaluation of the Katz-Thompson model for estimating the water permeability of cement-based materials from mercury intrusion porosimetry data. *Cem. Concr. Res.,* 24(3): 443–455.

[24] Ellison, A.H., R.B. Klemm, A.M. Schwartz, L.S. Grub, and D.A. Petrash. 1967. Contact angles of mercury on various surfaces and the effect of temperature. *J. Chem. Eng. Data*, 12(4): 607–609.

[25] Evans, R.B., G.M. Watson, and E.A. Mason. 1961. Gaseous diffusion in porous media at uniform pressure. *J. Chem. Phys.,* 35(6): 2076–2083.

[26] Friesen, W.I. and R.J. Mikula. 1987. Fractal dimensions of coal particles. *J. Colloid Interface Sci.,* 120(1): 263–271.

[27] Gao, Z. and Q. Hu. 2012. Using spontaneous water imbibition to measure building materials' effective permeability. *Spec. Topics Rev. in Porous Media- An Intern. J.,* 3(3): 209–213.

[28] Gao, Z. and Q. Hu. 2013. Estimating permeability using median pore-throat radius obtained from mercury intrusion porosimetry. *J. Geophys. Eng.,*10(2), 025014.

[29] Giesche, H. 2006. Mercury porosimetry: a general (practical) overview. *Part. Part. Syst. Charact.,* 23: 1–11.

[30] Gillham, R. W., M. L. J. Robin, D. J. Dytynyshyn, and H. M. Johnson. 1984. Diffusion of nonreactive and reactive solutes through fine-grained barrier materials. *Can.Geotech. J.,* 21: 541.

[31] Grathwohl, P. 1998. Diffusion in Natural Porous Media: Contaminant Transport, Sorption/Desorption and Dissolution Kinetics. Kluwer Academic Publishing, Boston, pp. 224.

[32] Graue, A. and M.A. Fernø. 2011. Water mixing during spontaneous imbibition at different boundary and wettability conditions. *J. Petrol. Sci. Eng.,* 78: 586–595.

[33] Hager, J. 1998. Steam Drying of Porous Media. Ph.D. Thesis, Department of Chemical Engineering, Lund University, Sweden.

[34] Handy, L.L. 1960. Determination of effective capillary pressures for porous media from imbibition data. *Trans. AIME.,* 219: 75–80.

[35] Hartmann, D.J. and E.A. Beaumont. 1999. Predicting reservoir system quality and performance. In: Beaumont, E.A., Foster, N.H. (Eds.), Exploring for Oil and Gas Traps: AAPG Treatise of Petroleum Geology: Handbook of Petroleum Geology. p. 9-1–9-154.

[36] Hassanizadeh, S.M. 1993. Toward an improved description of the physics of two-phase flow. *Adv. Water Res.,* 16: 53–67.

[37] Hazen, A. 1911. Discussion: Dams on sand foundations. *Trans. Amer. Soc. Civil Engrs.,* 73:199.

[38] Hilfer, R. 1998. Macroscopic equations of motion for two-phase flow in porous media. *Phys. Rev. E,* 58 (2): 2090–2096.

[39] Hu, Q., P. Persoff, and J.S.Y. Wang. 2001. Laboratory measurement of water imbibition into low-permeability welded tuff*. J. Hydrol.,* 242: 64–78.

[40] Hu, Q., R.P. Ewing, and S. Dultz. 2012. Low pore connectivity in natural rock. *J. Contam. Hydrol.,* 133: 76–83.

[41] Kast, W. and C.R. Hohenthanner. 2000. Mass transfer within the gas-phase of porous media. *Int. J. Heat Mass Transfer,* 43: 807–823.

[42] Katz, A.J. and A.H. Thompson. 1986. A quantitative prediction of permeability in porous rock. *Phys. Rev. B.,* 34: 8179–81.

[43] Katz, A.J. and A.H. Thompson. 1987. Prediction of rock electrical conductivity from mercury injection measurements. *J. Geophys. Res.,* 92(B1): 599–607.

[44] Kolodzie, S. Jr. 1980. Analysis of pore throat size and use of the Waxman-Smits equation to determine OOIP in Spindle Field. Colorado Society of Petroleum Engineers, 55th Annual Fall Technical Conference Paper 9382, 10p.

[45] Kumar, R. and B. Bhattacharjee. 2004. Assessment of permeation quality of concrete through mercury intrusion porosimetry. *Cem. Concr. Res.,* 34: 321-328.

[46] León, C.A.L. 1998. New perspectives in mercury porosimetry. *Adv. Colloid Interface Sci.,* 76-77: 341-372.

[47] Li, K. 2007. Scaling of spontaneous imbibition data with wettability included. *J. Contam. Hydrol.,* 89: 218–230.

[48] Li, K. and R.N. Horne. 2001. Characterization of spontaneous water imbibition into gas-saturated rocks. *SPE J,* 6 (4): 375-384.

[49] Loucks, R.G., and S.C. Ruppel. 2007. Mississippian Barnett Shale: Lithofacies and depositional setting of a deep-water shale-gas succession in the Fort Worth Basin, Texas. *Am. Assoc. Pet. Geol. Bull.,* 91(4): 579–601.

[50] Loucks, R.G., R.M. Reed, S.C. Ruppel, and D.M. Jarvie. 2009. Morphology, genesis, and distribution of nanometer-scale pores in siliceous mudstones of the Mississippian Barnett Shale. *J. Sediment. Res.,* 79: 848–861.

[51] Loucks, R.G., R.M. Reed, S.C. Ruppel, and U. Hammes. 2012. Spectrum of pore types and networks in mudrocks and a descriptive classification for matrix-related mudrock pores. *Am. Assoc. Pet. Geol. Bull.,* 96(6): 1071–1098.

[52] Lu, X. 1997. Application of the Nernst-Einstein equation to concrete. *Cem. Concr. Res.,* 27 (2): 293–302.

[53] Lu, X., M. Chen, and F. Yuan. 2000. Evaluation of concrete permeability by critical voltage. *Cem. Concr. Res.,* 30: 973–975.

[54] Ma, S. and N.R. Morrow. 1996. Relationships between porosity and permeability for porous rocks. SCA Conference Paper Number 9610.

[55] Ma, S., N.R. Morrow, and X. Zhang. 1997. Generalized scaling of spontaneous imbibition data for strongly water-wet systems. *J. Petrol. Sci. Eng.,* 18: 165–178.

[56] Makhanov, K., H. Dehghanpour, and E. Kuru. 2012. An experimental study of spontaneous imbibition in Horn River shales. SPE Canadian Unconventional Resources Conference, October 30 - November 1, Calgary, Alberta, Canada, DOI 10.2118/162650-MS.

[57] Mason, G., H. Fischer, N.R. Morrow, D.W. Ruth, and S. Wo. 2009. Effect of sample shape on counter-current spontaneous imbibition production vs time curves. *J. Petrol. Sci. Eng.,* 66: 83–97.

[58] Mattax, C.C. and J.R. Kyte. 1962. Imbibition oil recovery from fractured, water drive reservoirs. *SPE J.,* June: 177–184.

[59] Moore, C.A. and A. Alzayadi. 1975. Theoretical considerations of movements of gases around sanitary landfills. Report to U.S. EPA.

[60] Moro, F. and H. Böhni. 2002. Ink-bottle effect in mercury intrusion porosimetry of cement-based materials. *J. Colloid Interface Sci.,* 246: 135–149.

[61] Morrow, N.R. 1990. Wettability and its effect on oil recovery. *J. Petrol. Technol.,* 42(12): 1476–1484.

[62] Morrow, N.R. and G. Mason. 2001. Recovery of oil by spontaneous imbibition. *Curr. Opin. Colloid Interface Sci.,* 6: 321–337.

[63] Morrow, N.R., S. Ma, X. Zhou, and X. Zhang. 1994. Characterization of wettability from spontaneous imbibition measurements. Annual Technical Meeting, Jun 12 - 15, Calgary, Alberta, Canada, DOI 10.2118/94-47.

[64] Mu, D., Z. Liu, and C. Huang. 2008. Determination of the effective diffusion coefficient in porous media including Knudsen effects. *Microfluid. Nanofluid.,* 4: 257–260.

[65] Peng, S., Q. Hu, and S. Hamamoto. 2012. Diffusivity of rocks: Gas diffusion measurements and correlation to porosity and pore size distribution. *Water Resour. Res., 48,* W02507, doi:10.1029/2011WR011098.

[66] Picandet, V., A. Khelidj, and H. Bellegou. 2009. Crack effects on gas and water permeability of concretes. *Cem. Concr. Res.,* 39: 537–547.

[67] Pollard, W.G. and R.D. Present. 1948. On gaseous self-diffusion in long capillary tubes*. Phys. Rev.,* 73: 752–774.

[68] Purcell, W.R. 1949. Capillary Pressures-their measurement using mercury and the calculation of permeability there from American Institute of Mechanical Engineers. Petroleum Transactions: 39–48.

[69] Rezaee, M. R., A. Jafari, and E. Kazemzadeh. 2006. Relationships between permeability, porosity and pore throat size in carbonate rocks using regression analysis and neural networks. *J.Geophys.Eng.,* 3: 370–376.

[70] RILEM Recommendations. 1984. Absorption of water by immersion under vacuum, materials and structures. *RILEM CPC 11.3,* 101: 393–394.

[71] Rojas, E., M. Pérez-Rea, G. Gallegos, and J. Leal. 2012. A Porous Model for the Interpretation of Mercury Porosimetry Tests. *J. Porous Media,* 15(6): 517–530.

[72] Rolston, D.E. and P. Moldrup. 2002. Gas diffusivity. Methods of Soil Analysis: Physical Methods. Part 4. J. H. Dane and G. C. Topp, Soil Science Society of American, Inc., Madison, Wisconsin, pp. 1113–1139.

[73] Schmid, K.S. and S. Geiger. 2012. Universal scaling of spontaneous imbibition for water-wet systems. *Water Resour. Res.,* 48, W03507, doi:10.1029/2011WR011566.

[74] Seo, J., S. Kato, Y. Ataka, and Q. Zhu. 2005. Evaluation of effective diffusion coefficient in various building materials and absorbents by mercury intrusion porosimetry. The 10th International Conference on Indoor Air Quality and Climate.

[75] Shackelford, C.D. 1991. Laboratory diffusion testing for waste disposal-A review. *J. Contam. Hydrol.,* 7: 177–217.

[76] Shahri, M.P., M. Jamialahmadi, and S.R. Shadizadeh. 2012. New normalization index for spontaneous imbibition. *J. Petrol. Sci. Eng.,* 82–83: 130–139.

[77] Shi, D. and D.N. Winslow. 1985. Contact angle and damage during mercury intrusion into cement paste. *Cem. Concr. Res.,* 15: 645–654.

[78] Silin, D., Tad W. Patzek, and Sally M. Benson. 2009. A one-dimensional model of vertical gas plume migration through a heterogeneous porous medium. *Intern. J. Greenhouse Gas Control,* 3: 300–310.

[79] Slatt, R.M. and N.R. O'Brien. 2011. Pore types in the Barnett and Woodford gas shales: Contribution to understanding gas storage and migration pathways in fine-grained rocks. *Am. Assoc. Pet. Geol. Bull.,* 95(12): 2017–2030.

[80] Standnes, D.C. 2010. Scaling spontaneous imbibition of water data accounting for fluid viscosities. *J. Petrol. Sci. Eng.,* 73: 214–219.

[81] Sulucarnain, I., C.H. Sondergeld, and C.S. Rai. 2012. An NMR study of shale wettability and effective surface relaxivity. SPE Canadian Unconventional Resources Conference, October 30 - November 1, Calgary, Alberta, Canada, DOI 10.2118/162236-MS.

[82] Swanson, B.F. 1981. A simple correlation between permeabilities and mercury capillary pressures. *J. Pet. Technol.,* 33: 2498–2504.

[83] Takahashi, S. and A.R. Kovscek. 2010. Wettability estimation of low-permeability, siliceous shale using surface forces. *J. Petrol. Sci. Eng.,* 75: 33–43.

[84] Tiab, D. and E.C. Donaldson. 2004. Petrophysics - Theory and practice of measuring reservoir rock and fluid transport properties, Elsevier, Amsterdam.

[85] Tsakiroglou, C.D. and A.C. Payatakes. 2000. Characterization of the pore structure of reservoir rocks with the aid of serial sectioning analysis, mercury porosimetry and network simulation. *Adv. Water Resour.,* 23: 773–789.

[86] Washburn, E.W. 1921. Note on a method of determining the distribution of pore sizes in a porous materials. *Proc. Nat. Acad. Sci.,* 7: 115–116.

[87] Webb, P.A. 2001. An introduction to the physical characterization of materials by mercury intrusion porosimetry with emphasis on reduction and presentation of experimental data. Micromeritics Instrument Corporation.

[88] Westermarck, S., A.M. Juppo, L. Kervinen, and J. Yliruusi. 1998. Pore structure and surface area of mannitol powder, granules and tablets determined with mercury porosimetry and nitrogen adsorption. *Eur. J. Pharm. Biopharm.,* 46: 61–68.

[89] Zhang, P. and T. Austad. 2006. Wettability and oil recovery from carbonates: Effects of temperature and potential determining ions. *Colloids Surf.,* A 279: 179–187.

[90] Zhang, X., N.R. Morrow, and S. Ma. 1996. Experimental verification of a modified scaling group for spontaneous imbibition. *SPE RE,* Nov: 280–285.

[91] Zhao, H., N.B. Givens, and B. Curtis. 2007. Thermal maturity of the Barnett Shale determined from well-log analysis. *Am. Assoc. Pet. Geol. Bull.,* 91(4): 535–549.

[92] Zhou, J., G. Ye, and K. Breugel. 2010. Characterization of pore structure in cement-based materials using pressurization-depressurization cycling mercury intrusion porosimetry (PDC-MIP). *Cem. Concr. Res.,* 40: 1120–1128.

Biographical Information

Zhiye Gao obtained his Bachelor of Science degree in Geochemistry from Nanjing University in 2009. And after one-year's working at a Chinese mineral exploration company, he chose to further his doctorate education by joining Dr. Qinhong Hu's research group at the University of Texas at Arlington in 2010. His research focused on using multiple approaches to characterizing the pore structure of different reservoir rocks (including conventional and unconventional hydrocarbon reservoirs).